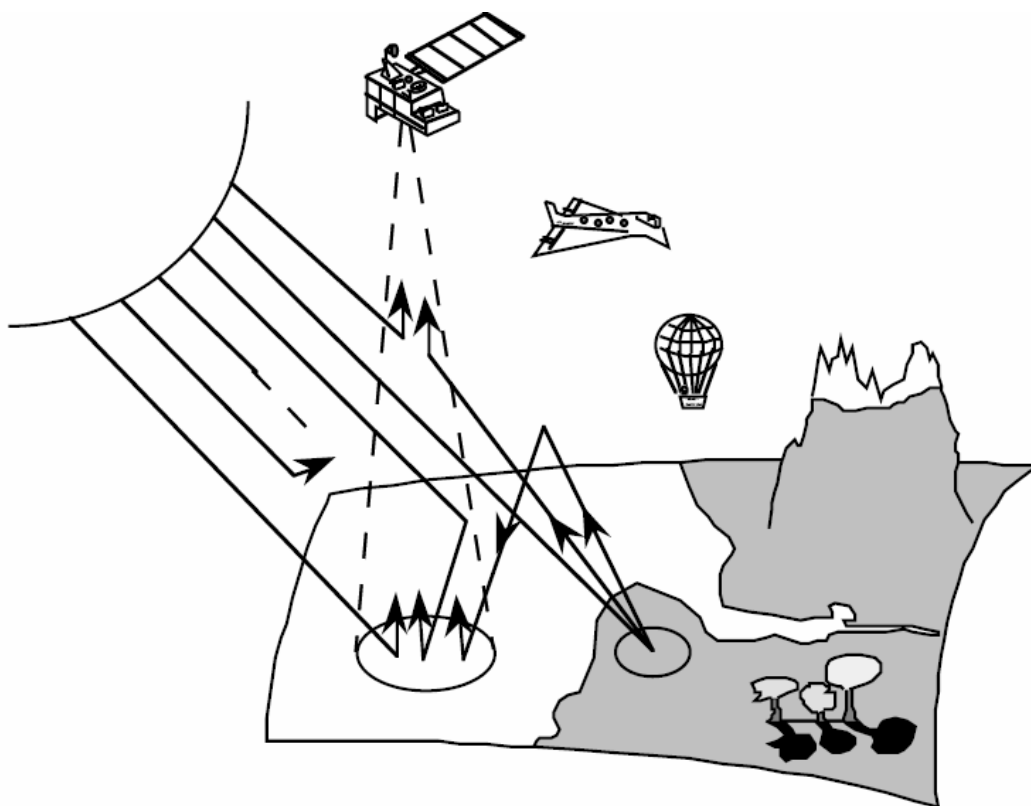


Second Simulation of a Satellite Signal in the Solar Spectrum - Vector (6SV)



Vermote E.^(1,*), D. Tanré⁽²⁾, J. L. Deuzé⁽²⁾, M. Herman⁽²⁾,
J. J. Morcrette⁽³⁾, and S. Y. Kotchenova⁽¹⁾

- (1) *Department of Geography, University of Maryland*
address for correspondence:
4321 Hartwick Road, Suite 209
College Park, MD 20740
- (2) *Laboratoire d'Optique Atmosphérique, URA CNRS 713*
Université des Sciences et Technologies de Lille
59655 Villeneuve d'Ascq Cédex, France
- (3) *European Centre for Medium Range Weather Forecast*
Shinfield Park, Reading
Berkshire RG2 9AX, United Kingdom

* Formerly affiliated with the Laboratoire d'Optique Atmosphérique

CONTENTS

| | |
|--|----|
| ABSTRACT | 3 |
| UPDATES | 4 |
| HISTORY | 5 |
| PHYSICAL BACKGROUND | 6 |
| DESCRIPTION OF ATMOSPHERIC EFFECTS IN SATELLITE OBSERVATIONS | 10 |
| 1. Absorbing effects | 10 |
| 2. Scattering effects | 11 |
| 2.1. Case of a Lambertian uniform target | 11 |
| 2.2. Environmental function | 14 |
| 2.3. Intrinsic atmospheric reflectance | 16 |
| 2.4. Airplane and elevated target simulations | 18 |
| 2.5. Directional effect of the target | 20 |
| 2.6. Atmospheric correction scheme | 22 |
| 3. Interaction between absorption and scattering effects | 23 |
| CONCLUSION | 26 |
| FIGURES | 27 |
| ACKNOWLEDGMENTS | 31 |
| APPENDIX | |
| I. Description of the computer code | 32 |
| II. Examples of inputs and outputs | 52 |
| III. Description of the subroutines | 56 |

ABSTRACT

This is the manual for a vector version of the 6S radiative transfer (RT) code (hereafter also referred to as 6SV), capable of accounting for radiation polarization. The manual presents a modified version of the previous scalar 6S manual. For the user's convenience, the format and style of this new manual have been kept as close as possible to those of the previous version.

6S - **Second Simulation of a Satellite Signal in the Solar Spectrum** - is a basic RT code used for the calculation of look-up tables in the MODIS (MODerate resolution Imaging Spectroradiometer) atmospheric correction algorithm. It enables accurate simulations of satellite and plane observations, accounting for elevated targets, modeling of a realistic molecular/aerosol/mixed atmosphere, use of Lambertian/anisotropic ground surfaces, and calculation of gaseous absorption. It is one of the most widely used, rigorously validated, and heavily documented RT codes known in the scientific remote-sensing community.

The latest updates on the code status (dated May 2005) include a public release of its vector version, 6SV1.0B. As its scalar predecessors, the vector version is based on the method of successive orders of scattering (SOS) approximations. The effects of polarization are included through the calculation of four components of the Stokes vector, characterizing the intensity of radiation, and perpendicular, parallel, and elliptical polarization. The accuracy of RT calculations can be varied by changing the number of calculation angles and layers. By default, 6SV1.0B uses the "standard accuracy" conditions which provide the user with a relative average accuracy of approximately 0.4-0.6%, compared to standard benchmarks and other RT codes.

UPDATES

The information on news and updates is posted on the 6S Web site at <http://6s.ltdri.org>. This site also contains pdf-files of relevant publications.

I. News

- 1) A special Web interface which can help an inexperienced user learn how to use the code and build necessary input files is available at the 6S Web site.
- 2) The paper “Validation of a vector version of the 6S radiative transfer code for atmospheric correction of satellite data. Part II: Homogeneous Lambertian and anisotropic surfaces”, by S.Y. Kotchenova, E.F. Vermote and P.A. Farris is submitted to *Applied Optics* in December, 2006.
- 3) 6SV is participating in the joint RT scalar/vector code comparison project, which the MODIS atmospheric correction group performs together with the NASA Goddard Space Flight Center, <http://rtcodes.ltdri.org>.

II. Changes

| Scalar version of 6S | Vector version of 6S |
|--|--|
| 1. Scalar (ignoring the effects of polarization) | 1. Vector (accounting for polarization) |
| 2. Fixed number of scattering angles (83), used for the specification of an aerosol phase function | 2. Ability to vary the number of scattering angles (up to 1000) |
| 3. 10 node wavelengths | 3. 20 node wavelengths |
| 4. Fixed number of calculation layers (26) and angles (48) | 4. Ability to change the number of calculation layers and angles |
| 5. Default exponential vertical aerosol profile | 5. Default exponential + user-defined (up to 50 layers in the height range 0-100 km) vertical aerosol profiles |

6. Several new subroutines, simulating measurements of the ALI, ASTER, ETM, HYPBLUE, VGT, and VIIRS instruments, have been integrated into the vector 6S. These subroutines were developed by Dr. T. Miura, University of Hawaii at Manoa, Honolulu, USA.

HISTORY

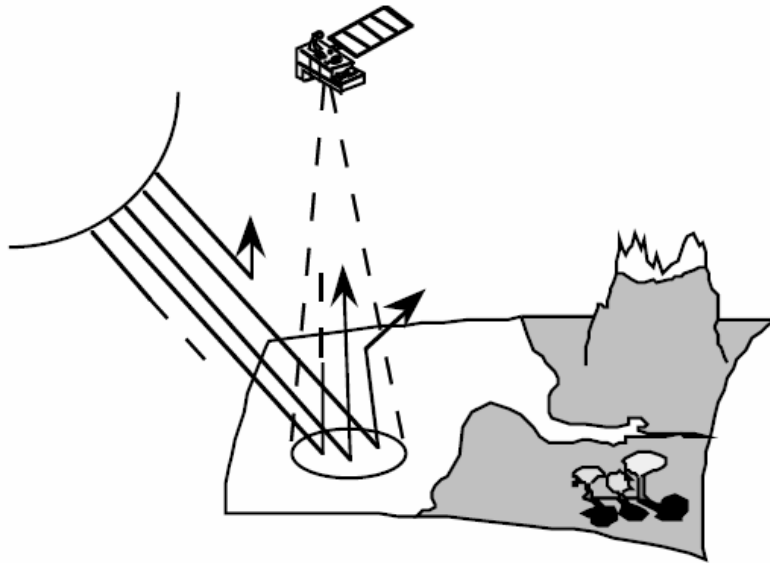
- July 1992** Development of the scalar 5S (Simulation of a Satellite Signal in the Solar Spectrum) RT code by le Laboratoire d'Optique Atmosphérique.
- July 1997** Release of a new improved version of the 5S code, called 6S (Second Simulation of a Satellite Signal in the Solar Spectrum). 6S becomes a basic RT code used for the calculation of look-up tables in the MODIS atmospheric correction algorithm.
- May 2005** Release of a vector version of 6S, capable of accounting for radiation polarization.
- October 2005** Organization of a joint scalar/vector RT code comparison project together with the NASA Goddard Space Flight Center.

PHYSICAL BACKGROUND

In the solar spectrum, sensors on meteorological or Earth remote sensing satellites measure the radiance reflected by the atmosphere-Earth surface system illuminated by the sun. This signal depends on the surface reflectance, but it is also perturbed by two atmospheric processes, the gaseous absorption and the scattering by molecules and aerosols.

In the ideal case (with no atmosphere), the solar radiation illuminates the surface. A fraction of the incoming photons is absorbed by the surface, whereas the remaining photons are reflected back to space. Therefore, the measured radiance directly depends on the surface properties: this radiance is the useful signal as much as it characterizes the actual surface reflectance.

In the actual case, the signal is perturbed by the atmosphere. Only a fraction of the photons coming from the target reaches the satellite sensor, typically 80% at 0.85 μm and 50% at 0.45 μm , so that the target seems less reflecting. The missing photons are lost through two processes: absorption and scattering.

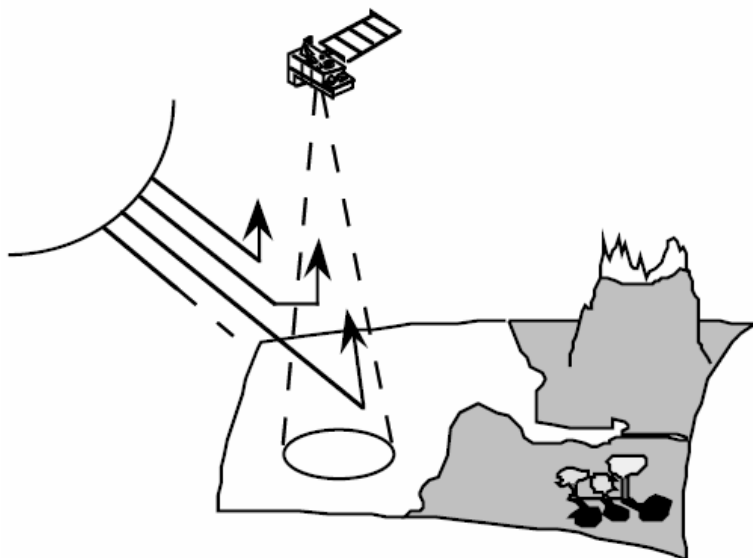


Some photons are absorbed by aerosols or atmospheric gases (principally O_3 , H_2O , O_2 , CO_2 , CH_4 , and N_2O). Generally, absorption by aerosols is small, and satellite sensor channels avoid the molecular absorption bands. Thus, in this study, the absorption effect is a correction factor. Nevertheless, we correct for the absorption as accurately as possible, so that the code can also be used to define new satellite sensor spectral channels. The absorption is computed using statistical band models with a 10 cm^{-1} resolution.

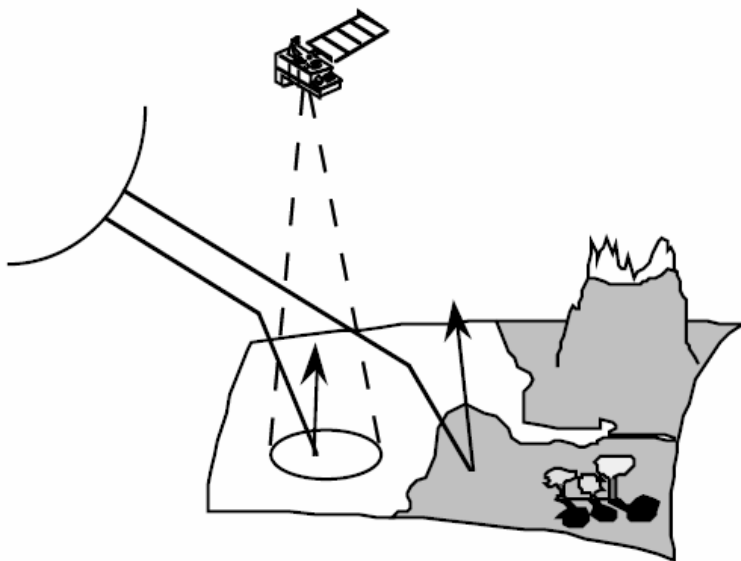
While some photons are absorbed, others are scattered. The interaction with molecules or non-absorbing aerosols is elastic, and the photons are immediately re-emitted in a direction other than the incident one. After one or several such scattering processes, these photons leave the atmosphere and must be counted in the budget of photons reaching the satellite sensor. However, their paths are more complex than the previous direct paths, as explained hereafter.

First, let us consider the photons coming from the sun and scattered by the atmosphere on the Sun-surface path:

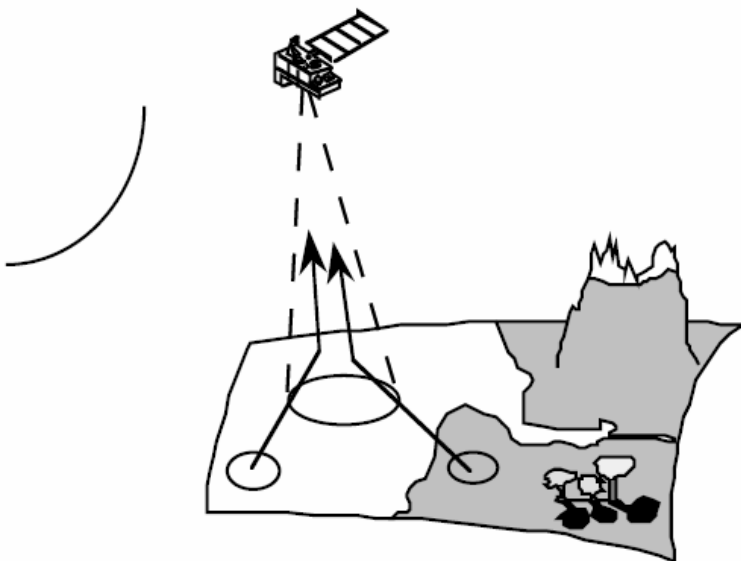
- Some of them do not reach the surface and are backscattered toward space. They take part in our radiative balance. This signal is an interference term; it does not carry any information about the target.



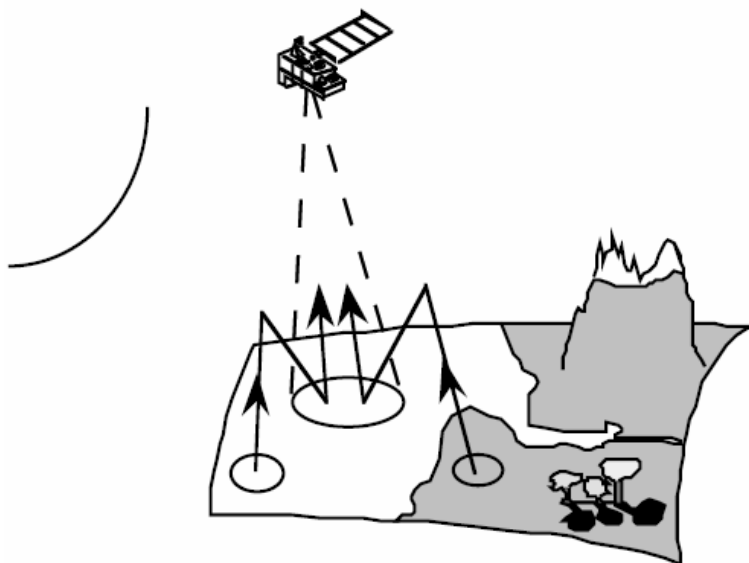
- The remaining photons contribute to the illumination of the ground by the way of scattered paths and compensate the attenuation of the direct solar paths. This diffuse component has therefore to be considered in the useful signal.



In a second step, let us consider the photons reflected by the surface and scattered by the atmosphere on the surface-satellite path. By the same process, a fraction will be scattered toward the sensor. This component has to be carefully considered. If the surface is uniform, it is a useful component, but if the surface has a patchy structure, this term will introduce environmental effects (or perturbation).



Finally, a fraction of the photons reflected by the surface will be backscattered by the atmosphere to the surface and will create a third component of its illumination. It is the trapping effect: the photons successively interact with the surface and the atmosphere but, generally, the convergence is fast and after one or two interactions, the phenomenon can be neglected.



From this qualitative description, we can then infer a modeling of the atmospheric effects based upon:

- an accurate estimation of the absorption by atmospheric gases,
- a complete treatment of the scattering processes,
- and an approximation for the interaction between the two processes.

DESCRIPTION OF ATMOSPHERIC EFFECTS IN SATELLITE OBSERVATIONS

1. Absorbing effects

In the solar spectrum the atmospheric gaseous absorption is principally due to:

- oxygen (O_2);
- ozone (O_3);
- water vapor (H_2O);
- carbon dioxide (CO_2);
- methane (CH_4);
- nitrous oxide (N_2O).

O_2 , CO_2 , CH_4 , and N_2O are assumed constant and uniformly mixed in the atmosphere, H_2O and O_3 concentrations depend on the time and the location. The latter two are the most important gases in our study.

Gases absorb the radiation by changes of rotational, vibrational or electronic states. The variations of rotational energy are weak and correspond to the emission or absorption of photons of weak frequency, which are then located in the microwave or far-infrared range. The vibrational transitions correspond to greater energy typical for the near infrared spectrum. They can also take place with rotational transitions and then give rise to vibrational-rotational bands. Lastly, electronic transitions correspond to more important energy and give rise to absorption or emission bands in the visible and the ultra-violet range. Since these transitions occur at discrete values, the absorption coefficients vary very quickly with the frequency and present a very complex structure.

Once the position, intensity and shape of each line in an absorption band are known, the absorption can then be exactly computed using line-by-line integrations. Such a model requires a very large computational time which makes it necessary to use an equivalent band model. We have divided the solar spectrum into spectral intervals of 10 cm^{-1} width using HITRAN database. This width allows a good description of the spectral variations of transmission and overlapping between absorption bands of different gases. Moreover, this allows enough absorption lines to be contained in order that the transmission models remain well adapted to the problem.

We chose two random exponential band models, *Goody* (1964) for H_2O and *Malkmus* (1967) for the other gases. When several gases present absorption bands, we set the total transmission equal to the product of each gas transmission.

A complete description of the statistical models is given in Appendix III (subroutine ABSTRA). Here we present the results for each gas between 0.25 μm and 4 μm for the US-1962 standard atmosphere model and the sun at the nadir (air mass is 1.0). These results are depicted in Fig. I-1 to I-6.

The H_2O contribution (Fig. I-1) affects mainly wavelengths greater than 0.7 μm . On the other hand, O_3 presents a significant absorption between 0.55 and 0.65 μm and limits the earth observations at wavelengths less than 0.35 μm (Fig. I-2). The CO_2 contribution occurs beyond 1 μm , but more weakly than H_2O and only perturbing the water vapor windows (Fig. I-3). The O_2 influence is limited to a very strong band about 0.7 μm (Fig. I-4). The CH_4 presents two absorption bands at 2.3 and 3.35 μm (Fig. I-6). Finally, the N_2O contribution appears in two bands at 2.9 and 3.9 μm (Fig. I-5).

In summary, we have, in the solar spectrum, good atmospheric windows for terrestrial observations by satellites:

- in the visible: between 0.40 and 0.75 μm
- in the near and middle infrared: at about 0.85, 1.06, 1.22, 1.60, 2.20 μm .

Figures I-7 to I-14 display these windows.

2. Scattering effects

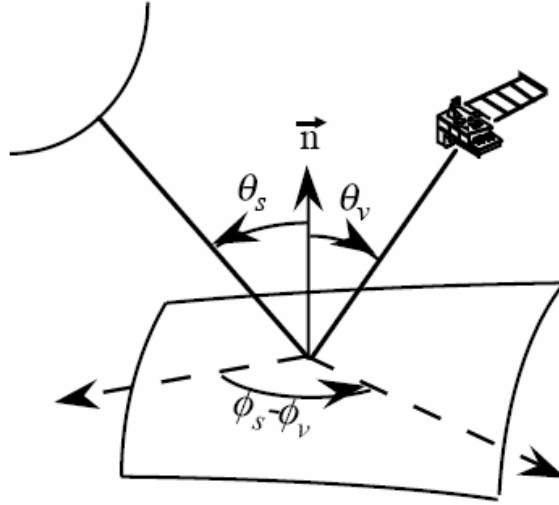
2.1. Case of a Lambertian uniform target

In the first step, assuming that the surface is of uniform Lambertian reflectance and the atmosphere is horizontally uniform and various, the measured quantities will be expressed in terms of equivalent reflectance, ρ^* defined as:

$$\rho^* = \frac{\pi L}{\mu_s E_s} \quad (1)$$

where L is the measured radiance, E_s is the solar flux at the top of the atmosphere, $\mu_s = \cos(\theta_s)$, and θ_s is the sun zenith angle.

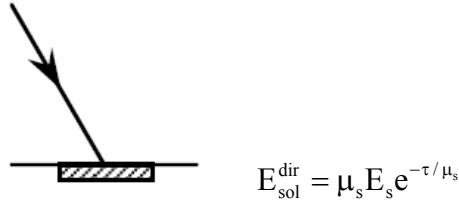
The optical thickness of the atmosphere will be noted τ , the viewing direction will be referenced by the zenith angle θ_v and the azimuth angle ϕ_v , and the sun angles by θ_s and ϕ_s . ρ_t will be the reflectance of the target. Absorption problems will not be considered in this part.



It is convenient to express the signal received by the satellite as a function of successive orders of radiation interactions in the coupled surface-atmosphere system.

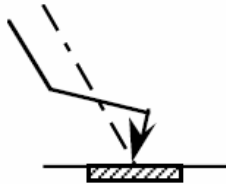
For the surface illumination, we have by decreasing magnitudes:

- the downward direct solar flux attenuated by the atmosphere E_{sol}^{dir}



$$E_{sol}^{dir} = \mu_s E_s e^{-\tau/\mu_s}$$

- the downward diffuse solar irradiance E_{sol}^{diff} , independent from surface properties and noted by a diffuse transmittance factor $t_d(\theta_s)$ defined as



$$t_d(\theta_s) = \frac{E_{sol}^{diff}(\theta_s)}{\mu_s E_s}$$

- a second scattered flux due to the trapping mechanism, which depends on the environment of the target and corresponds to the successive reflections and scattering between the surface and the atmosphere. If the spherical albedo of the atmosphere is noted S , we can write this term as:



$$\left[e^{-\tau/\mu_s} + t_d(\theta_s) \right] \left[\rho_t S + \rho_t^2 S^2 + \dots \right]$$

The total normalized illumination at the surface level is then written

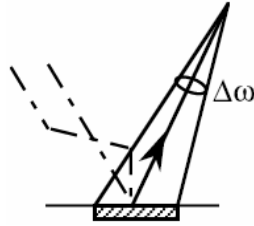
$$T(\theta_s) / [1 - \rho_t S], \quad (2)$$

where $T(\theta_s)$ is the total transmittance:

$$T(\theta_s) = e^{-\tau/\mu_s} + t_d(\theta_s) \quad (3)$$

At the satellite level, the radiance results from

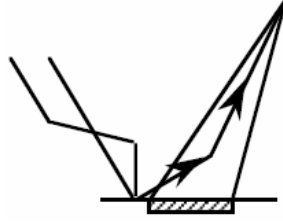
- the contribution of the total (direct plus diffuse) solar radiation reflected by the surface and directly transmitted from the surface to the sensor, expressed by $e^{-\tau/\mu_v}$ with $\mu_v = \cos(\theta_v)$



- the intrinsic atmospheric radiance expressed in terms of reflectances by function $\rho_a(\theta_s, \theta_v, \phi_s, \phi_v)$



- the contribution of the environment which reflects the total (direct + diffuse) downward flux, the photons reaching the sensor by scattering; we note this new atmospheric diffuse transmittance as $t'_d(\theta_v)$



So, the apparent reflectance ρ^* at the satellite level can be expressed as

$$\rho^*(\theta_s, \theta_v, \phi_s - \phi_v) = \rho_a(\theta_s, \theta_v, \phi_s - \phi_v) + \frac{T(\theta_s)}{1 - \rho_t S} (\rho_t e^{-\tau/\mu_v} + \rho_t t'_d(\theta_v)) \quad (4)$$

According to the reciprocity principle, the functions $t_d(\theta_s)$ and $t'_d(\theta_v)$ are identical and ρ^* can be rewritten as

$$\rho^*(\theta_s, \theta_v, \phi_s - \phi_v) = \rho_a(\theta_s, \theta_v, \phi_s - \phi_v) + \frac{\rho_t}{1 - \rho_t S} T(\theta_s) T(\theta_v) \quad (5)$$

with

$$T(\theta_v) = e^{-\tau/\mu_v} + t_d(\theta_v) \quad (6)$$

2.2. Environmental function

Let us assume that the surface reflectance is now not uniform. First, we will consider a small target M of reflectance $\rho_c(M)$ with an uniform environment of reflectance $\rho_e(M)$. In this case, Eq.(4) remains interesting by its formalism: it gives the weight of each reflectance and ρ^* can be now written as

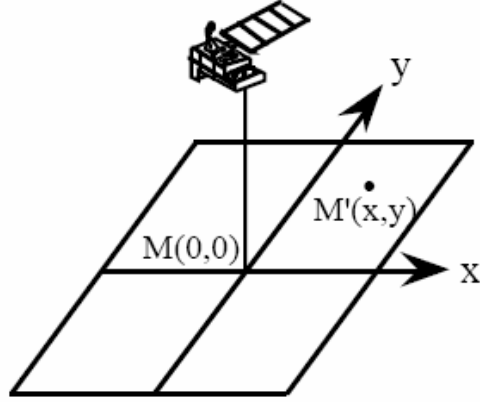
$$\rho^*(\theta_s, \theta_v, \phi_s - \phi_v) = \rho_a(\theta_s, \theta_v, \phi_s - \phi_v) + \frac{T(\theta_s)}{1 - \rho_e S} (\rho_c(M) e^{-\tau/\mu_v} + \rho_e(M) t_d(\theta_v)) \quad (7)$$

If we now consider a patchy structure, we keep the same formalism as in Eq.(7), we only have to define a new environment reflectance noted $\langle \rho(M) \rangle$ which represents a spatial average of each pixel reflectance over the whole surface.

$$\rho^*(\theta_s, \theta_v, \phi_s - \phi_v) = \rho_a(\theta_s, \theta_v, \phi_s - \phi_v) + \frac{T(\theta_s)}{1 - \langle \rho(M) \rangle S} (\rho_c(M) e^{-\tau/\mu_v} + \langle \rho(M) \rangle t_d(\theta_v)) \quad (8)$$

This spatial average must be weighted by an atmospheric function which takes into account the efficiency of a point M' according to the distance from the point M , so $\langle \rho(M) \rangle$ will be given by:

$$\langle \rho(M) \rangle = \frac{1}{t_d(\theta_v)} \int_{-\infty}^{+\infty} \int_{-\infty}^{+\infty} \rho'(x, y) e(x, y, \theta_v) dx dy \quad (9)$$



where

- M is the origin of the x, y coordinate system ;
- $\rho'(x,y)$ is the reflectance of the point $M'(x,y)$;
- $e(x,y,\theta_v)$ is the contribution to the diffuse transmission $t_d(\theta_v)$ per unit area of an isotropic unit source placed at $M'(x,y)$.

The use of the same average reflectance $\langle \rho(M) \rangle$ for the high orders of interaction (that is the geometrical series) is incorrect but reasonable because in most cases the contribution from these terms does not exceed 10-15% of the contribution of the first order term.

If we restrict the modeling to the case of vertical observations (or nearly, $\theta_v < 30^\circ$), Eq. (9) can be written

$$\langle \rho(M) \rangle = \int_0^{2\pi} \int_0^\infty \rho'(r, \phi) r p(r) dr d\phi \quad (10)$$

with

$$r p(r) = \frac{r e(r, \phi, 0)}{t_d(0)}, \quad (11)$$

where (r, ϕ) are the polar coordinates of a given surface point with object pixel M at the origin. For off-nadir observation, we will see in the subroutine ENVIRO how to handle the problem.

Actually, it is impossible to solve this problem exactly, using Eq. (10) because of the computational time involved. Generally, we can define a characteristic size r of the target whose reflectance can be assumed uniform. By the same way, we can compute the environment reflectance ρ_e reflected by a simple arithmetical mean and we estimate $\langle \rho(M) \rangle$ in the following manner.

Let us consider a circular target of radius r and reflectance ρ_c surrounded by a homogeneous surface of reflectance ρ_e . Eq.(10) becomes

$$\langle \rho(M) \rangle = \rho_c F(r) + (1 - F(r)) \rho_e \quad (12)$$

with

$$F(r) = 2\pi \int_0^r r' p(r') dr' \quad (13)$$

which gives the relative contribution to $\langle \rho(M) \rangle$ of surface points not farther than a distance r apart from the origin.

2.3. Intrinsic atmospheric reflectance

For the intrinsic atmospheric reflectance observed over a black target, $\rho_r + \rho_a$ is written here as the sum of aerosols and Rayleigh contributions. This decomposition is not valid at short wavelengths (less than $0.45\mu\text{m}$) or at large sun and view zenith angles.

2.3.1. Rayleigh

Atmospheric reflectance

For isotropic scattering, *Chandrasekhar* (1960) showed how solutions derived for small optical thicknesses may be extended to larger values of τ . He expressed the atmospheric reflectance $\rho_a(\mu_s, \mu_v, \phi_v - \phi_s)$ as

$$\rho_a(\mu_s, \mu_v, \phi_v - \phi_s) = \rho_a^1(\mu_s, \mu_v, \phi_v - \phi_s) + (1 - e^{-\tau/\mu_s})(1 - e^{-\tau/\mu_v}) \Delta(\tau) \quad (14)$$

where $\rho_a^1(\mu_s, \mu_v, \phi_v - \phi_s)$ is the single-scattering contribution and the second term accounts roughly for higher orders of scattering.

In 6S, we use this approach to compute the molecular scattering reflectance.

Transmission function

The transmission function refers to the normalized flux measured at the surface. There are several approximate expressions based on the two-stream methods for computing the transmitted flux. The accuracy of these expressions depends on the scattering properties of the atmospheric layer (thick or thin clouds or aerosols) and on the geometrical conditions. The delta-Eddington method, which has been proved to be well suited for our conditions, has been selected. Since molecular scattering is conservative ($\omega_0=1$) and the anisotropy factor g is equal to zero, we may write

$$T(\mu) = \frac{[2/3 + \mu] + [2/3 - \mu]e^{-\tau/\mu}}{4/3 + \tau} \quad (15)$$

where μ is the cosine of the solar and/or observational zenith angle and τ is the optical thickness.

Spherical albedo

In conservative cases such as molecular scattering, the spherical albedo s is given by

$$s = 1 - \int_0^1 \mu T(\mu) d\mu \quad (16)$$

where $T(\mu)$ has been given in Eq.(15). Using Eqs.(15) and (16), the spherical albedo can be written as

$$s = \frac{1}{4 + 3\tau} [3\tau - 4E_3(\tau) + 6E_4(\tau)] \quad (17)$$

where $E_3(\tau)$ and $E_4(\tau)$ are exponential integrals for the argument τ .

2.3.2. Aerosols

For the aerosols, the optical scattering parameters were computed using pre-defined models, Continental, Maritime, Urban or user's model based on a mixture of 4 basic components: dust-like, oceanic, water-soluble, and soot. In 6S, these options are still usable but we added three new models, the biomass burning smoke, background desert and stratospheric, and we also offer the user the possibility of making up their own aerosol model (4 components maximum, see the description of the subroutine MIE for details).

In 5S, the scattering properties pertaining to the aerosol layer were calculated using the *Sobolev* (1975) approximation for the reflectance, *Zdunkowsky et al.* (1980) for the transmittance and a semi-empirical formula for the spherical albedo. This provided the user having limited computing resources with a fast approximation. One drawback to using these approximations was that the accuracy of the computations could be off by a few percent in reflectance units, especially at large view and sun angles or high optical thicknesses. In addition, these approximations could be completely insufficient to handle the integration of the downward radiance field with non-Lambertian ground conditions, a problem in simulating BRDF. The new scheme used to compute the (aerosol + Rayleigh) coupled system relies on the Successive Orders of Scattering method. The accuracy of such a scheme is better than 10^{-4} in reflectance units. Other improvements on the 5S model include an atmosphere divided into 13 layers which

enables exact simulations of airborne observations; the downward radiation field is computed for a quadrature of 13 Gaussian emerging angles which will provide the necessary inputs for BRDF simulations (see 2.5).

2.4. Airplane and elevated target simulations

2.4.1. Elevated target simulation

For a target not at sea level, Eq.(5) is modified as follows:

$$\rho^*(\theta_s, \theta_v, \phi_s - \phi_v, z_t) = T_g(\theta_s, \theta_v, z_t) \left[\rho_r(z_t) + \rho_a + \frac{\rho_t}{1 - S(z_t)\rho_t} T(\theta_v, z_t) T(\theta_s, z_t) \right] \quad (18)$$

The target altitude or pressure indicates the amount of scatterers above the target (molecules and aerosols) and the amount of gaseous absorbents. The target altitude z_t is handled in the following manner: After the atmospheric profile and the target altitude or pressure are selected, a new atmospheric profile is computed by stripping out the atmospheric level above target altitude and interpolating if necessary. This way, an exact computation of the atmospheric parameters is computed, without any kind of approximation which will account for coupled pressure-temperature effect on absorption.

Gaseous absorption

In most cases, only the integrated content may be modified. The user still has the option to enter the total amount of H_2O and O_3 , but in this case the quantity entered must be representative of the level measured or estimated at the target location. The influence of target altitude on T_g has been evaluated. The absorption effect by O_3 is not sensitive to target altitude, because the ozone layer is located in the upper levels of the atmosphere, the variation of the altitude of the target does not modify this effect. The target's altitude has an important effect on the absorption by H_2O because most of the water vapor is located in the lower atmosphere. However, the exact sensitivity of the target's altitude on water vapor absorption cannot be generalized because the water vapor profile is variable.

Scattering function

The effect of target altitude on molecular optical thickness is accounted for in 6S. A good approximation, if needed, is to consider that τ_r is proportional to the pressure at target level. As the amount and types of aerosols are entered as parameters, the aerosol characteristics implicitly

depend on target altitude because they are measured at target location.

2.4.2. Airborne sensor simulation

In the case of a sensor inside the atmosphere (aircraft simulation), Eq (5) is modified as follows:

$$\rho^*(\theta_s, \theta_v, \phi_s - \phi_v, z) = T_g(\theta_s, \theta_v, z) \left[\rho_r(z) + \rho_a(z) + \frac{\rho_t}{1 - S(z)\rho_t} T(\theta_v, z) T(\theta_s, z) \right] \quad (19)$$

Gaseous absorption

Gaseous absorption is computed with a technique similar to the one used in the case of a target not at sea level. Only, the upward path is modified: the atmosphere levels above the sensor altitude are stripped, so the computation is done only to the altitude of the sensor (interpolation of the atmospheric profile is conducted if necessary). The effect of altitude on gaseous transmission has been computed. For visible wavelength ranges, O₃ absorption on the target-sensor path is no longer accounted for due to the fact these molecules are located above most aircraft sensors. H₂O absorption is very dependent on sensor altitude up to 4 km. If the observed channel is sensitive to water vapor absorption (as it is in the case of AVHRR channel 2) we recommend that additional measurements of water vapor should be taken from the aircraft. An additional option has been set up in 6S for this purpose and enables the user to enter ozone and water vapor contents (as well as aerosol content) for the portion of the atmosphere located under the plane.

Atmospheric reflectance and transmittance

In most cases the simple approximation "equivalent atmosphere" for atmospheric reflectance and transmittance is sufficiently accurate, i.e.,

$$\rho_r(z) \cong \rho_r(z = \infty, \tau_r(0 \rightarrow z)) \quad (20)$$

$$T(\tau_r, \theta_v, z) \cong T(\tau_r(0 \rightarrow z), \theta_v, z = \infty) \quad (21)$$

which means that computations are performed for optical thicknesses corresponding to the integration between the surface and the sensors.

In 6S, the computation is performed exactly by defining one of the multiple layers used in the Successive Orders of Scattering as the altitude of the sensor. This enables exact computation of both reflectance and transmission terms for a realistic mixing between aerosol and Rayleigh.

2.4.3. Non-uniform target

In 5S, the case of a non-homogeneous target is solved using Eqs. (8) and (12) where the function $F(r)$ is defined as

$$F(r) = \frac{t_d^r(\mu_v)F^r(r) + t_d^a(\mu_v)F^a(r)}{t_d(\mu_v)} \quad (22)$$

The problem of a target not at sea level, as long as we consider that the target and environment are at the same altitude, can be solved just by modifying the Rayleigh optical thickness.

In the case of aircraft observations, first we have to take into account the reduction of the amount of scatters under the plane. This can be done just by adjusting $t_d^r(\mu_v)$ and $t_d^a(\mu_v)$ to $t_d^r(z, \mu_v)$ and $t_d^a(z, \mu_v)$. Once this has been done, the principal part of the effect accounted for is a global reduction (factor 5-10 for an altitude of flight of 6 km) of the "environment effect". The second effect is the dependence of $F^r(r)$ and $F^a(r)$ upon altitude of the sensor. Monte Carlo simulation of $F^r(r)$ and $F^a(r)$ have been performed for different altitudes of the sensor (0.5,... 12 km) and included in 6S as a database. In the case of a plane observation, the closest simulated altitudes are used to interpolate the environment function at the aircraft altitude.

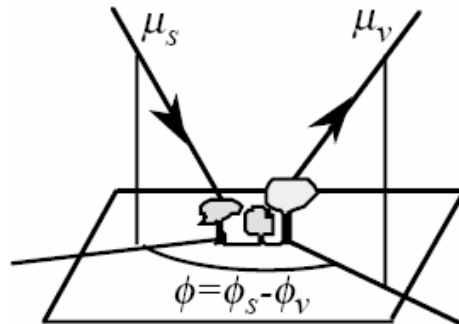
2.5. Directional effect of the target

2.5.1. BRDF

In 6S, the coupling of BRDF with the atmosphere is addressed; the contribution of the target to the signal at the top of the atmosphere is decomposed as the sum of four terms:

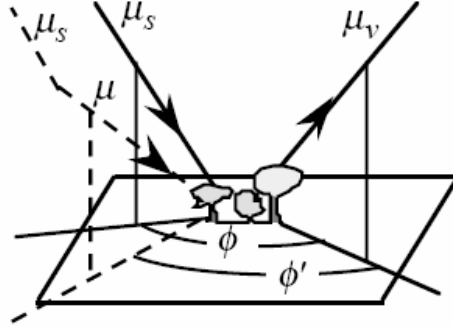
- the photons directly transmitted from the sun to the target and directly reflected back to the sensor

$$e^{-\tau/\mu_s} \cdot \rho_t(\mu_s, \mu_v, \phi) e^{-\tau/\mu_v} \quad (23)$$



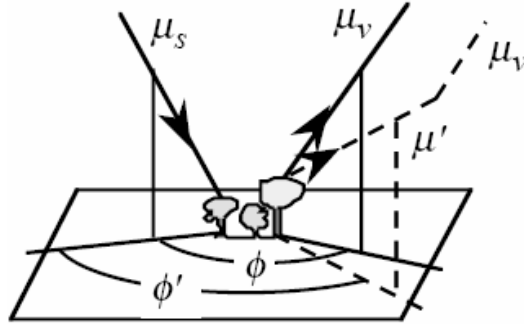
- the photons scattered by the atmosphere, then reflected by the target and directly transmitted to the sensor,

$$t_d(\mu_s) \bar{\rho}_t(\mu_s, \mu_v, \phi) e^{-\tau/\mu_v} = t_d(\mu_s) \frac{\int_0^{2\pi} \int_0^1 \mu L^\downarrow(\mu_s, \mu, \phi') \cdot \rho_t(\mu, \mu_v, \phi' - \phi) d\mu d\phi'}{\int_0^{2\pi} \int_0^1 \mu L^\downarrow(\mu_s, \mu, \phi') d\mu d\phi'} e^{-\tau/\mu_v} \quad (24)$$



- the photons directly transmitted to the target but scattered by the atmosphere on their way to the sensor,

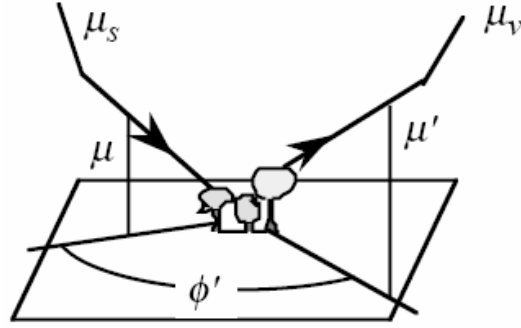
$$t_d(\mu_v) \bar{\rho}_t'(\mu_s, \mu_v, \phi) e^{-\tau/\mu_s} = t_d(\mu_v) \bar{\rho}_t(\mu_v, \mu_s, \phi) e^{-\tau/\mu_s} \quad (25)$$



- the photons having at least two interactions with the atmosphere and one with the target:

$$t_d(\mu_v) t_d(\mu_s) \bar{\rho}_t + \frac{T_{R+A}(\mu_s) T_{R+A}(\mu_v) S(\bar{\rho}_t)^2}{1 - S \bar{\rho}_t} \quad (26)$$

with $\bar{\rho}_t = \overline{\rho_t'(\mu_s, \mu_v, \phi)}$



In 6S, the first three contributions are computed exactly using the downward radiation field as given by the Successive Orders of Scattering method. The contribution which involves at least two interactions between the atmosphere and the BRDF (Eq.(26)) is approximated by taking $\bar{\rho}_t$ equal to the hemispherical albedo of the target

$$\bar{\rho}_t \cong \int_0^1 \mu_s \int_0^{2\pi} \int_0^1 \mu \rho_t(\mu_s, \mu_v, \phi' - \phi) d\mu_v d\phi d\mu_s \quad (27)$$

This approximation is required because the exact computation needs a double integration which would result in very long computation times. It is in addition justified by the limited impact on the total signal of this last contribution mitigated by $t_d(\mu_s) \cdot t_d(\mu_v)$ and also because the radiation field after one interaction tends to be isotropic.

2.5.2. Sunlint

The solar radiation directly reflected by the water surface is computed exactly with the Snell-Fresnel laws. For a rough sea surface, the reflection is conditioned by the wind and its description is by necessity a statistical one. Thus, the model surface can be computed numerically by many facets whose slopes are described by a Gaussian distribution (*Cox & Munk*, 1954). In 6S, this slope distribution is considered anisotropic (depending upon wind direction). Operationally, the scheme to compute the reflection by the sunlint is identical to BRDF ones.

2.6. Atmospheric correction scheme

An input parameter allows activating atmospheric correction mode. In this case, the ground is considered to be Lambertian, and as the atmospheric conditions are known, the code retrieves the atmospherically corrected reflectance value ρ_{ac} that will produce the reflectance (or the radiance) equal to the apparent reflectance ρ_i^* (Eq. (1)) (or apparent radiance) entered as input. Following Eq. (5), ρ_{ac} be determined as:

$$\rho_{ac}(\theta_s, \theta_v, \phi_s - \phi_v) = \frac{\rho_{ac}'}{1 + \rho_{ac}'} \quad (28)$$

with

$$\rho_{ac}' = \frac{\frac{\rho_i^*(\theta_s, \theta_v, \phi_s - \phi_v)}{Tg} - \rho_a(\theta_s, \theta_v, \phi_s - \phi_v)}{T(\theta_s)T(\theta_v)} \quad (29)$$

where ρ_i^* is the input parameter and where all the others parameters are computed in the atmospheric conditions described by the user.

3. Interaction between absorption and scattering effects

The atmospheric radiation depends on atmospheric transmittances which can be modified by the contribution of absorbing gases. The gaseous absorption must therefore be computed for each scattering path. We can simplify the problem and separate the two processes.

Let us consider the O₃ gas. It is localized at altitudes where molecules and aerosols are sparse, so the incident and reflected radiation go through the O₃ layer with nearly no scattering. So, we compute the atmospheric radiation ρ^* without accounting for O₃. We modify the signal by the only direct transmittance which corresponds to the twofold paths:

$$Tg_{O_3}(\theta_s, \theta_v, U_{O_3}), \quad (30)$$

where U_{O_3} is the absorber amount.

In the case of H₂O and CO₂, the absorption bands occur in the near and middle infrared. In this range, the molecular scattering becomes negligible and we only have to take into account the aerosol scattering. Some simulations, made for realistic atmospheres, show that beyond 0.850 μ m, the 1st and 2nd scattering constitute almost the whole diffuse radiation. Because the aerosol phase function has a large forward scattering, the diffuse paths are not completely separate from direct paths and we shall consider that the influence of CO₂ or H₂O upon scattered flux is the same as for direct solar flux. So the diffuse and transmitted flux will both be reduced by the factor

$$Tg_{H_2O}(\theta_s, \theta_v, U_{H_2O})Tg_{CO_2}(\theta_s, \theta_v, U_{CO_2}) \quad (31)$$

For O₂, the absorption is highly localized and presents a very narrow band, so we take into account this gas by using the same approach:

$$Tg_{O_2}(\theta_s, \theta_v, U_{O_2}) \quad (32)$$

We have checked our approximation with a simulation in the visible Meteosat spectral band. This band is large enough (0.35-1.10 μm) to include both scattering effects and water vapor absorption. To amplify the coupling effect, we have taken a tropical atmosphere model (H_2O content is about 4 g/cm^2) and a continental aerosol model with large optical depth ($\tau_{0.55\mu\text{m}} = 1$). For $\Delta_v = 20 \text{ cm}^{-1}$, we have:

| μ_s | $T^{\text{exact}}(\theta_s)$ | $T^{\text{est}}(\theta_s)$ |
|---------|------------------------------|----------------------------|
| 1.0 | 0.837 | 0.843 |
| 0.5 | 0.692 | 0.693 |
| 0.1 | 0.401 | 0.363 |

Table 1. Estimation of the accuracy of our approximation.

The comparison between exact computations and results obtained from our approach is reported in the above table for three solar angles. Except for a grazing incidence ($\mu_s = 0.1$), we have good agreement and the error related to this approximation is smaller than one percent.

For atmospheric reflectance, the problem is slightly different. The diffuse paths are not close to the direct paths. The photons are scattered at large angles away from the forward direction. For O_3 , the same approximation is still justified because it is based upon the weak interaction between the two processes. For H_2O , the scale height is comparable to the scale height of aerosols, while CO_2 is uniformly mixed. Therefore, for these two gases our approximation is less valid but remains sufficiently accurate as long as the gaseous absorption is small, i.e., in the atmospheric windows.

For getting the maximum uncertainties resulting from the approximation, we consider 2 extreme cases in 6S: the water vapor above the aerosol layer (maximum absorption, see Eq. (33-a) for $i=3$), the water vapor under the aerosol layer (minimum absorption, see Eq. (33-a) for $i=1$); and an average case where we consider that half of the water vapor present in the atmosphere absorbs the aerosol path radiance (see Eq. (33-a) for $i=2$). Thus, the satellite signal is written

$$\begin{aligned} \rho_{TOA}^{i=1,3}(\theta_s, \theta_v, \phi_s - \phi_v) = & Tg^{OG}(\theta_s, \theta_v) \left[\rho_R + (\rho_{R+A} - \rho_R) Tg^{H_2O}(\theta_s, \theta_v, \frac{i-1}{2} U_{H_2O}) \right. \\ & \left. + T^\downarrow(\theta_s) T^\uparrow(\theta_v) \frac{\rho_s}{1 - S\rho_s} Tg^{H_2O}(\theta_s, \theta_v, U_{H_2O}) \right], \end{aligned} \quad (33-a)$$

where Tg^{OG} refers to the gaseous transmission for gases other than water vapor, Tg^{H_2O} refers to

H₂O absorption and $\rho_{R+A} - \rho_R$ is an estimate of the aerosol intrinsic reflectance. For each case, we compute the top-of-atmosphere reflectance, so the uncertainty due to the vertical distribution of aerosol versus water vapor can be considered. Tg^{OG} is computed on the sun-target-satellite direct paths using

$$Tg^{OG}(\theta_s, \theta_v) = \prod_{i=1}^8 Tg_i(\theta_s, \theta_v, U_i). \quad (33-b)$$

CONCLUSIONS

An accurate analytical expression of the reflectance measured by a satellite-sensor or a sensor aboard an aircraft has been established.

- In the case of Lambertian and uniform surface, we completely separate the surface-atmosphere system and define three atmospheric functions:
 - the intrinsic atmospheric signal component,
 - the total transmittance,
 - the spherical albedo.
- The coupled BRDF-atmosphere is accounted for according to the same scheme by definition of mean angular reflectances which depend on atmospheric properties.
- In case of a non-uniform ground, we have defined a spatial average reflectance which remains slightly dependent on atmospheric properties by the definition of the function $F(r)$. This function allows us to take into account the main blurring atmospheric effect for non-uniform surfaces.

In all cases, it is possible to consider elevated targets.

The absorption by atmospheric gases is computed separately as a simple multiplicative factor. The solar spectrum is divided into spectral intervals of 10 cm^{-1} width.

In addition, a scheme of atmospheric correction is available.

The computational aspect of our work is now detailed in the following appendixes:

- Appendix I: General description of the computer code.
- Appendix II: Examples of inputs and outputs.
- Appendix III: Complete description of the subroutines.

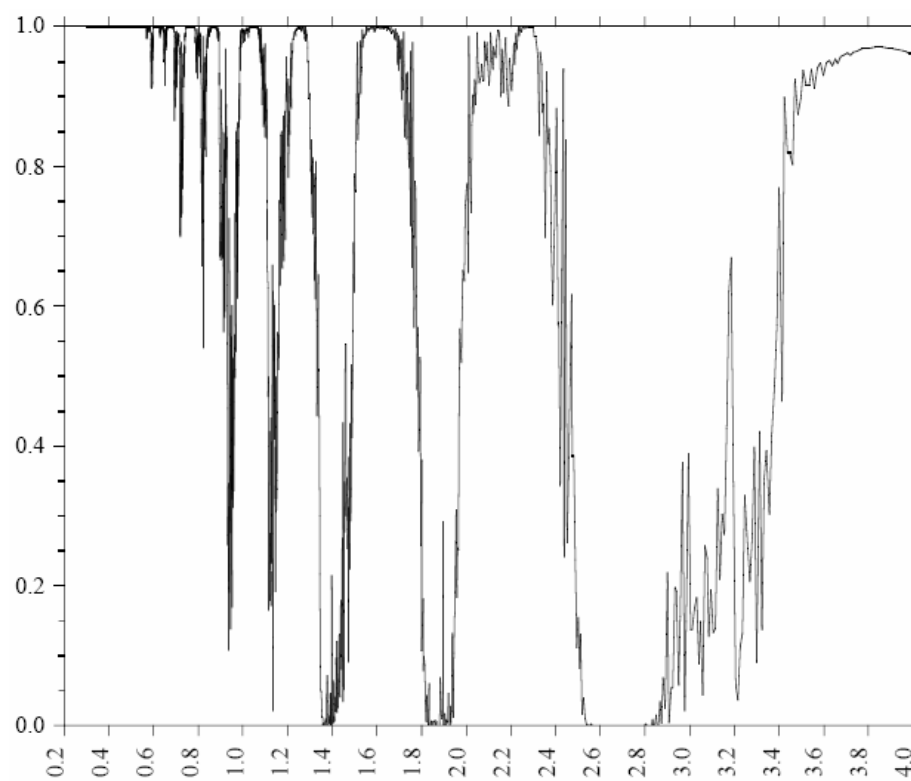


Fig. I-1. Spectral transmittance of H₂O.

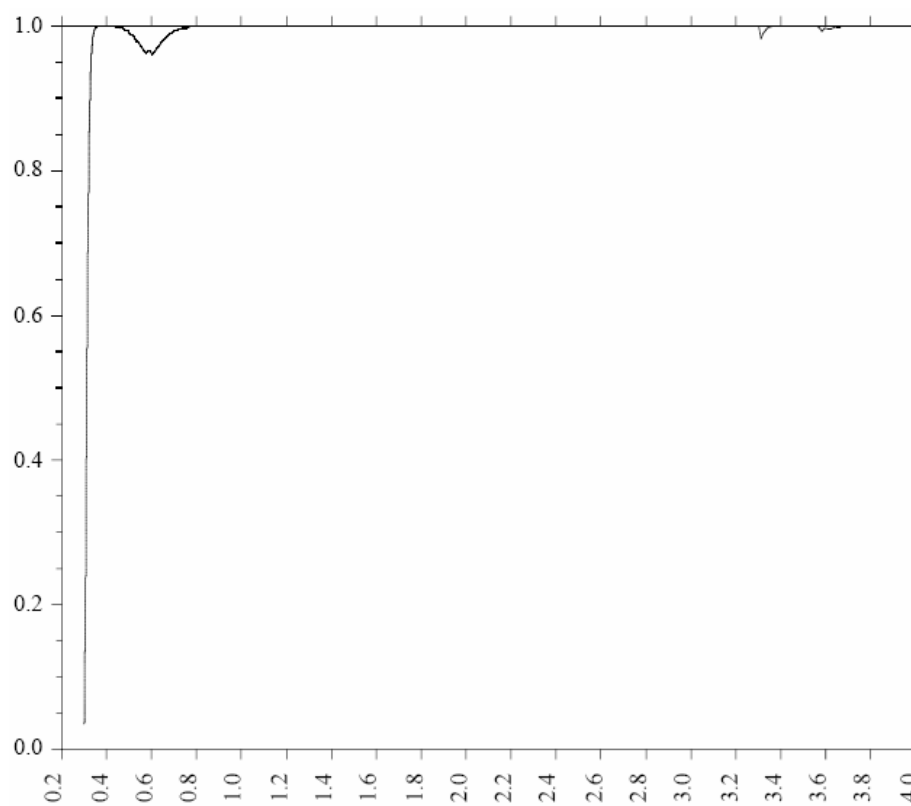


Fig. I-2. Spectral transmittance of O₃.

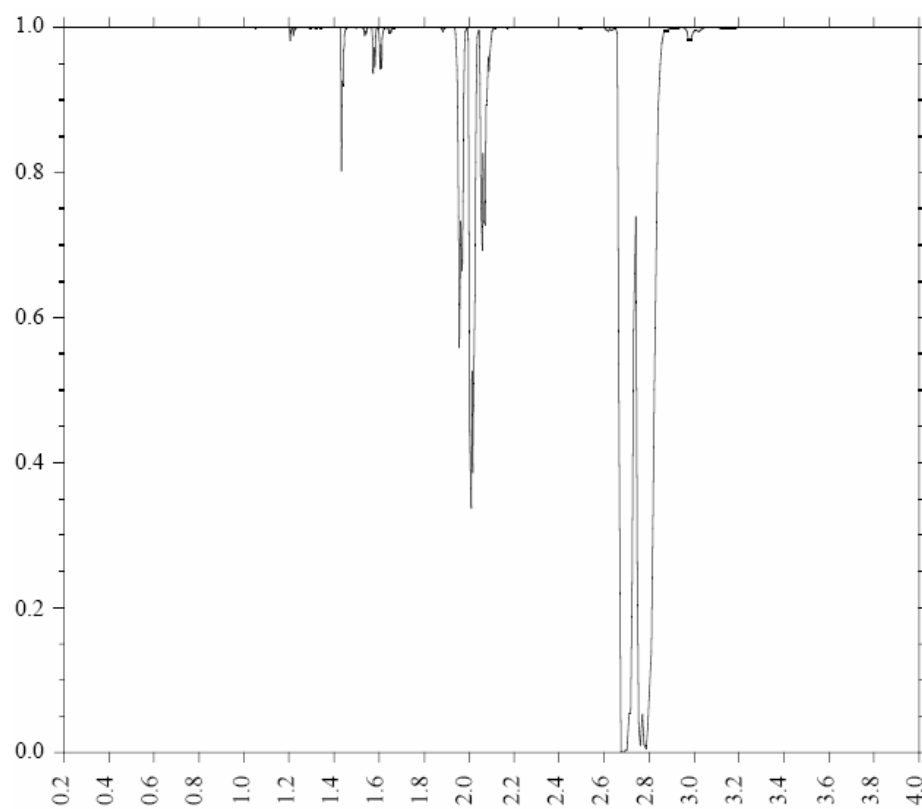


Fig. I-3. Spectral transmittance of CO₂.

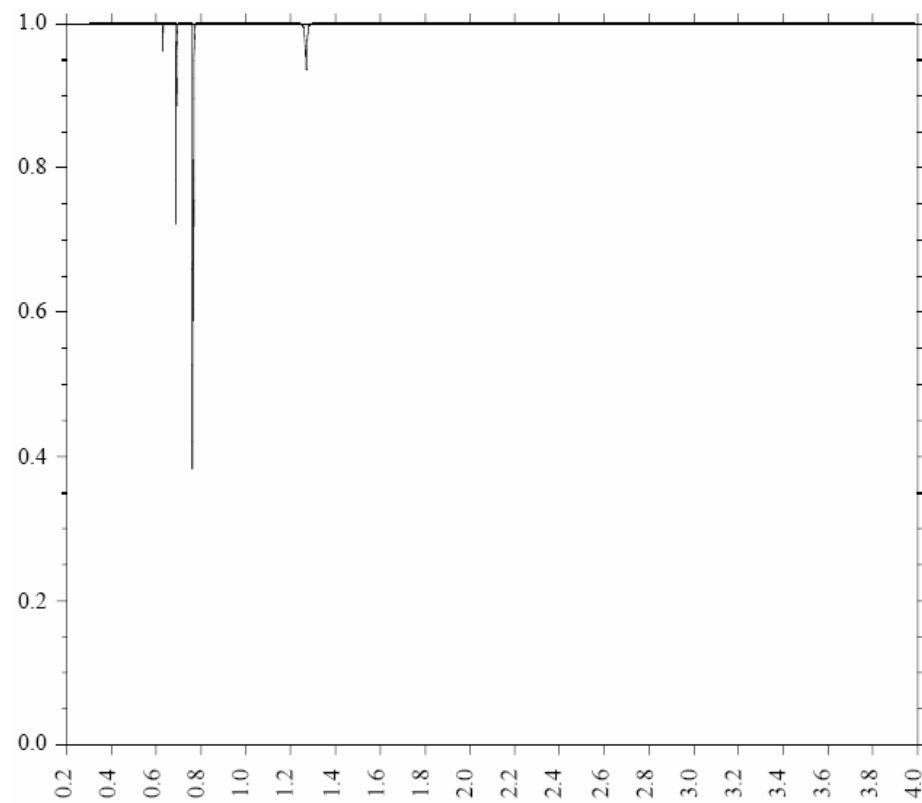


Fig. I-4. Spectral transmittance of O₂.

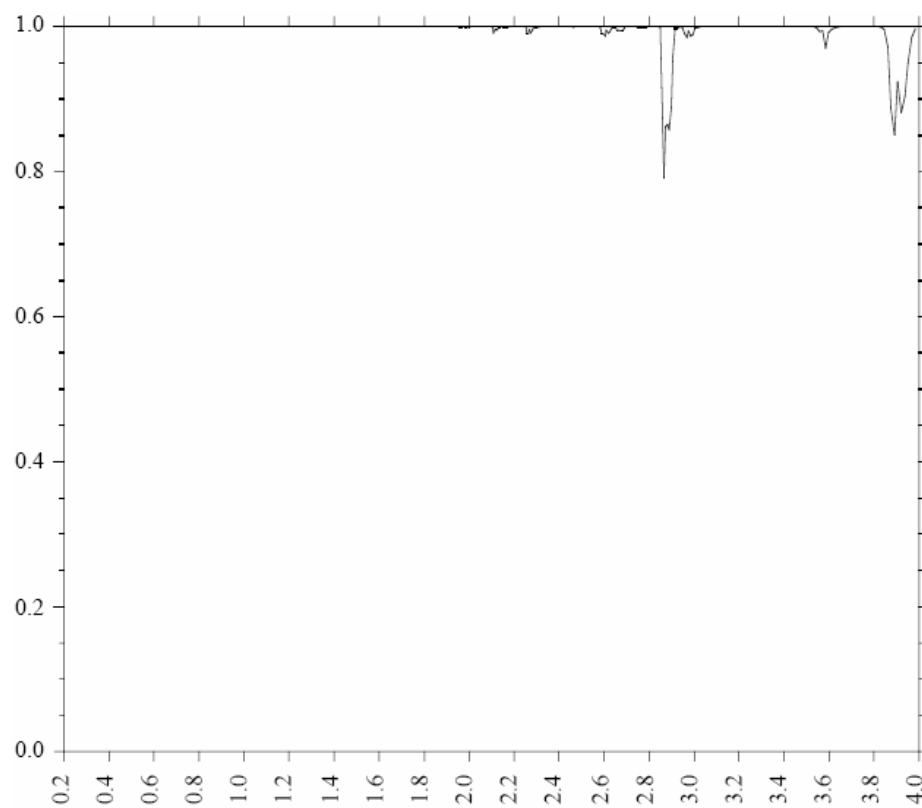


Fig. I-5. Spectral transmittance of N₂O.

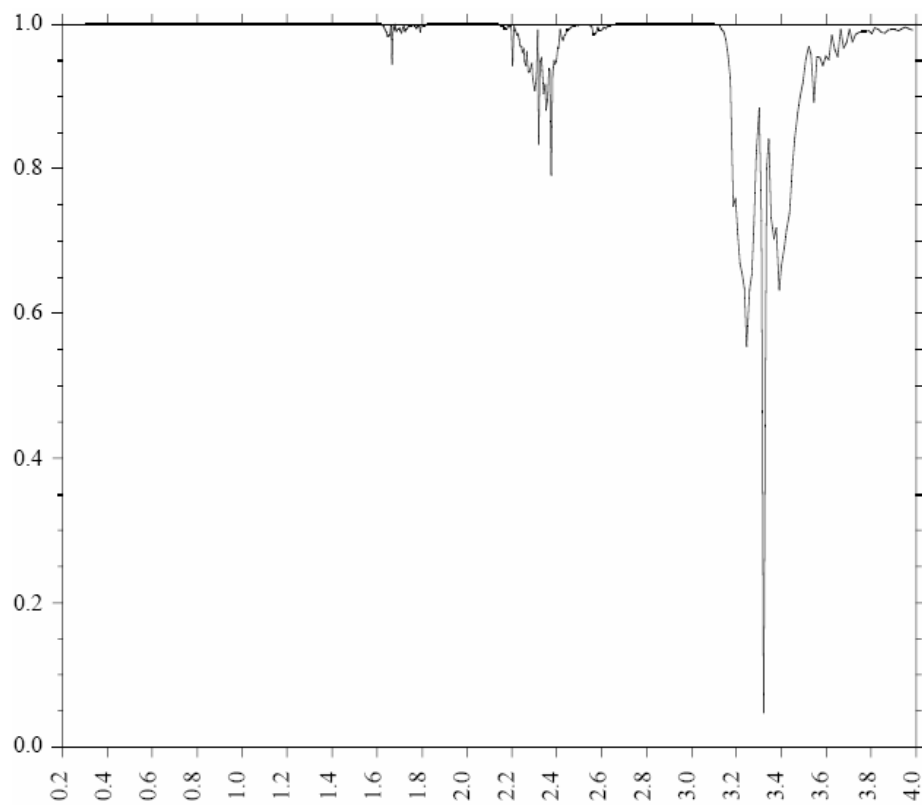


Fig. I-6. Spectral transmittance of CH₄.

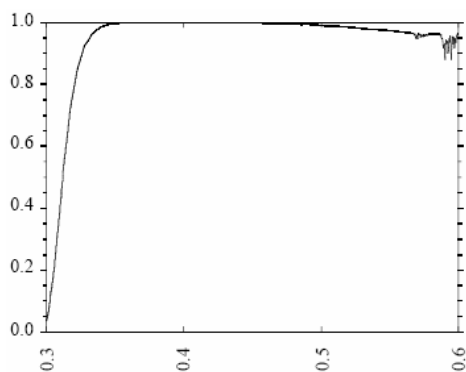


Fig. I-7. Atmospheric window at 0.40 μm .

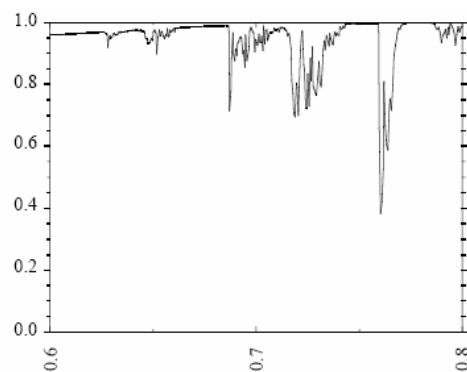


Fig. I-8. Atmospheric window at 0.75 μm .

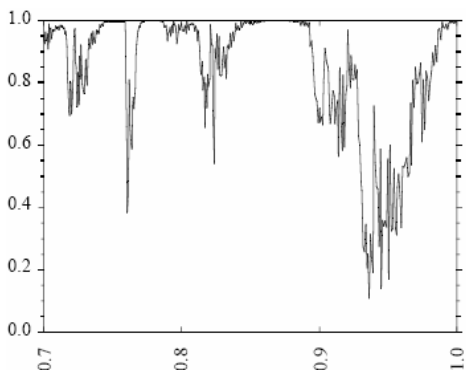


Fig. I-9. Atmospheric window at 0.85 μm .

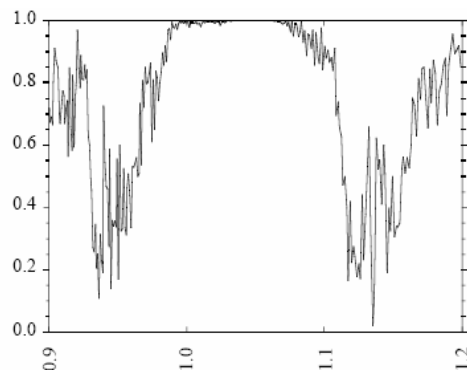


Fig. I-10. Atmospheric window at 1.06 μm .

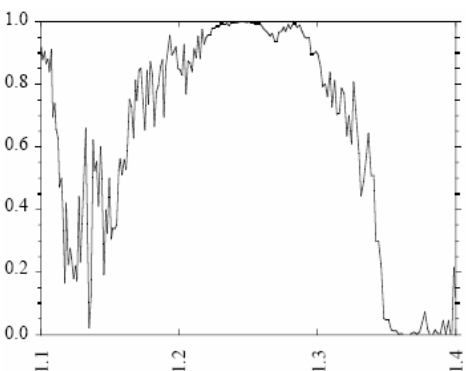


Fig. I-11. Atmospheric window at 1.22 μm .

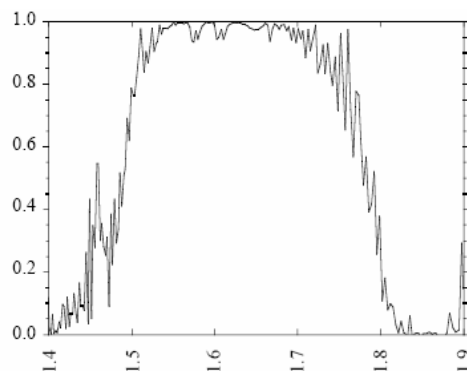


Fig. I-12. Atmospheric window at 1.60 μm .

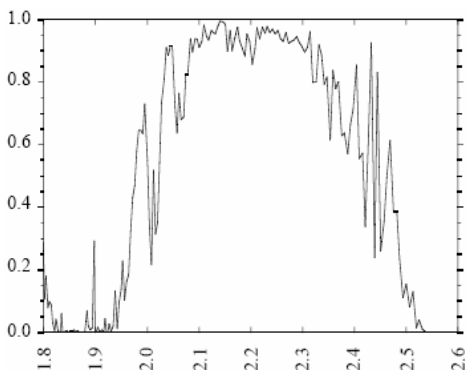


Fig. I-13. Atmospheric window at 2.20 μm .

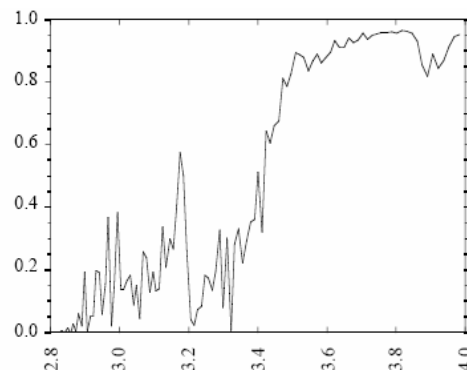


Fig. I-14. Atmospheric window at 3.70 μm .

ACKNOWLEDGEMENTS

Scalar 6S:

The authors would like to thank Nazmi Saleous from the GIMMS group for his help in putting together this manual, and Lorraine Remer from Code 923 for reading the first draft of the manual and helping us improve it. They are very grateful to Dr. Compton Tucker and Dr. Chris Justice from GSFC/UMD for the logistic support essential to the realization of 6S. Finally, special thanks to all Beta testers of the code and in particular to Phil Teillet from the Canadian Centre for Remote Sensing for his interesting and useful remarks.

Vector 6S:

We authors would like to thank student Jose Roa and Philip Farris from the University of Maryland for their help with the preparation of this modified version of the manual. They also want to thank Dr. Tomoaki Miura from the University of Hawaii at Manoa for developing six satellite subroutines.

APPENDIX I: DESCRIPTION OF THE COMPUTER CODE

This code predicts a satellite signal between 0.25 and 4.0 μm assuming cloudless atmosphere. Let us recall that the apparent reflectance at the satellite level for Lambertian surface can be written,

$$\rho'(\theta_s, \theta_v, \phi_v) = t_g(\theta_s, \theta_v) \left\{ \rho_a(\theta_s, \theta_v, \phi_v) + \frac{T(\theta_s)}{1 - \langle \rho(M) \rangle S} [\rho_c(M) e^{-\tau/\mu_v} + \langle \rho(M) \rangle t_d(\theta_v)] \right\}$$

This formalism takes into account the main atmospheric effects, gaseous absorption by H_2O , O_2 , CO_2 and O_3 , scattering by molecules and aerosols and a ground surface. The general flow chart for 6SV program is reported in Fig. A-1.

The following input parameters are necessary:

- geometrical conditions,
- atmospheric model for gaseous components,
- aerosol model (type and concentration),
- spectral condition,
- ground reflectance (type and spectral variation).

At each step, you can either select some proposed standard conditions or define your own conditions. More details are given in Figs. A-2 to A-9. Let us note that the satellite navigation is done by a rough calculation from the nominal characteristics of the satellite orbit. It is obvious that, without anchor points, the localization is not very accurate.

From these data, we compute the scattering atmospheric functions, at ten wavelengths which are well distributed over the solar spectrum (Fig. A-11). At any wavelength, we interpolate from these values by assuming the spectral dependence

$$f(\lambda) = f(\lambda_0) \left(\frac{\lambda}{\lambda_0} \right)^{-\alpha}$$

and compute the apparent reflectance from the first equation (Fig. A-10).

We have reported in Fig. A-12 the general outputs and the optional ones.

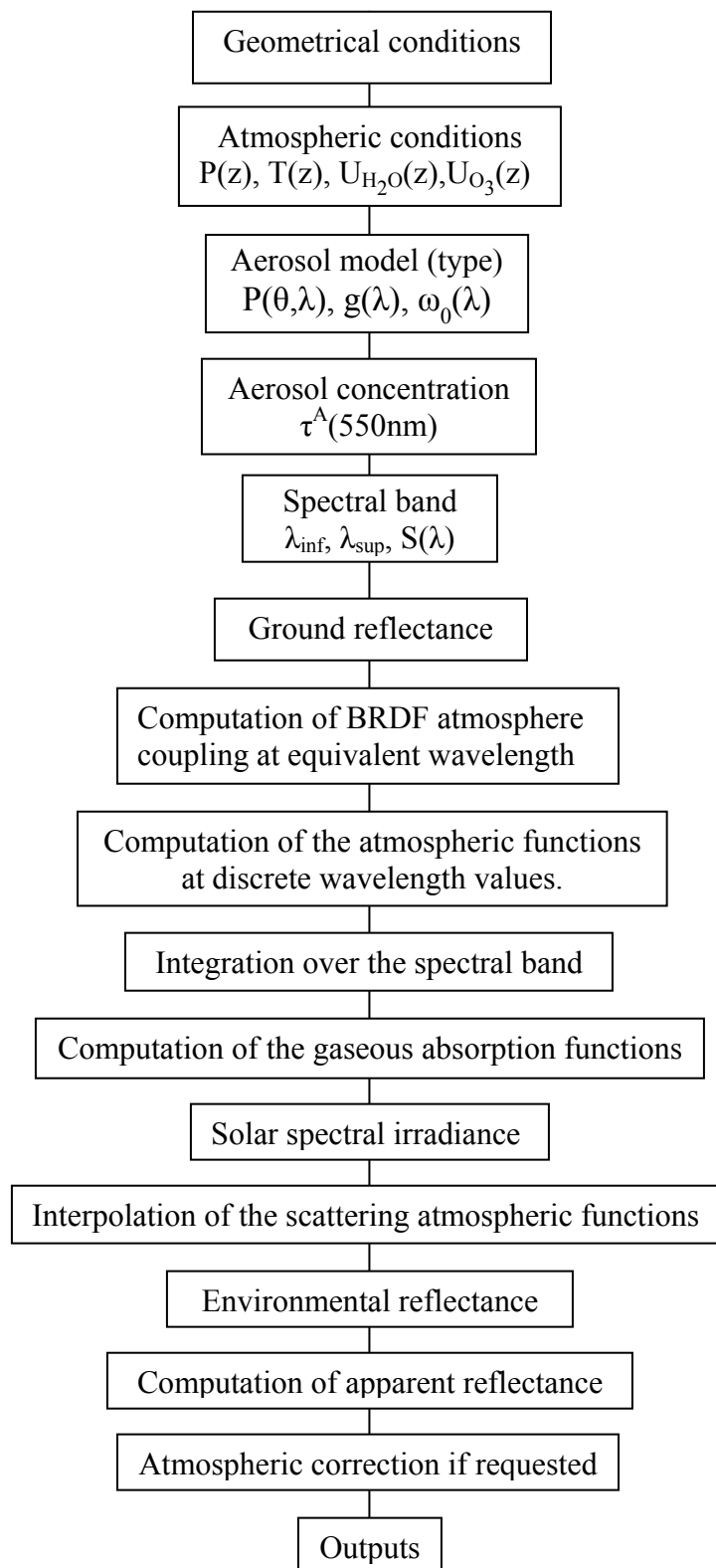


Fig. A-1. General flow chart of 6SV computations.

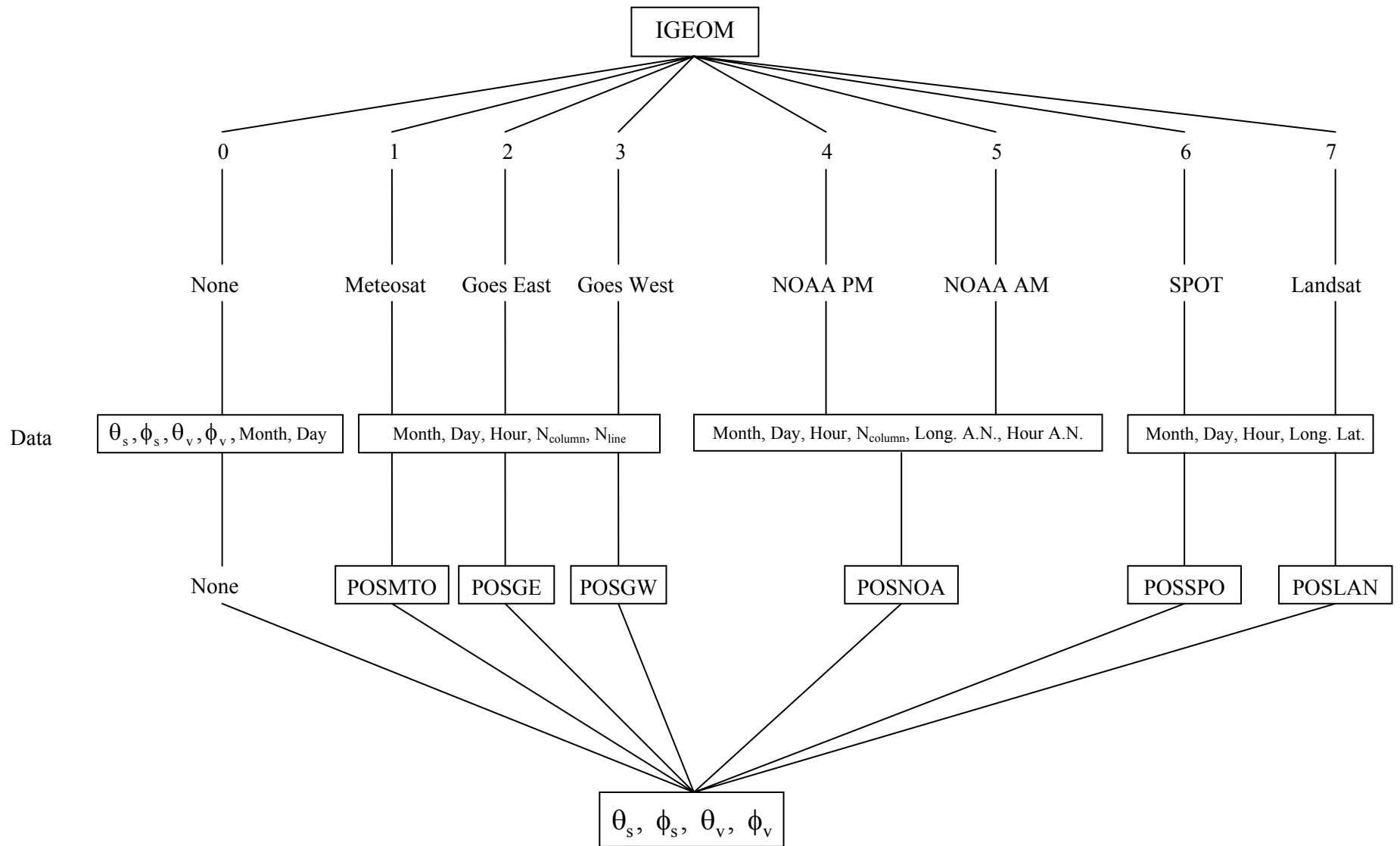


Fig. A-2. Detailed flow chart for geometrical conditions.

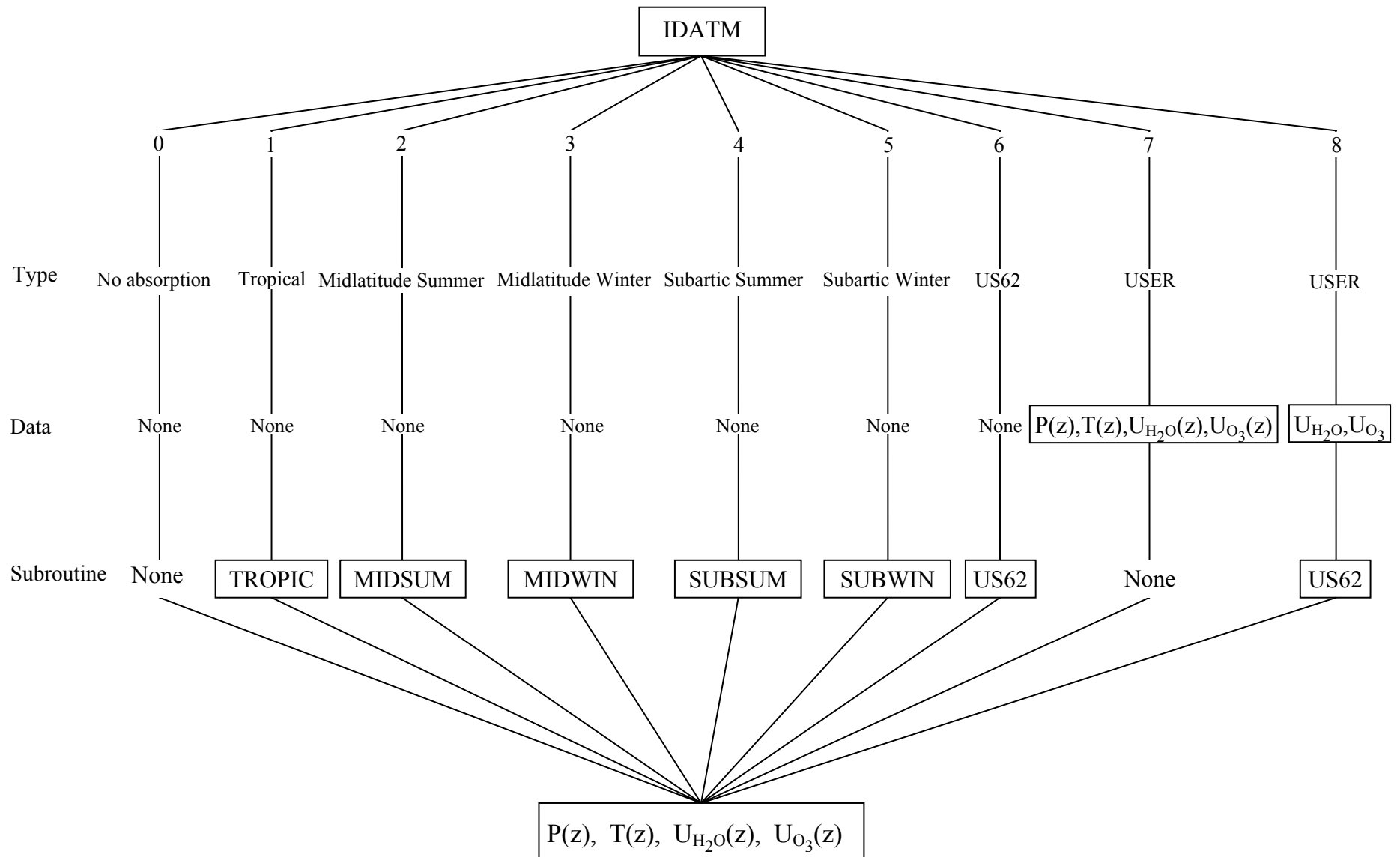


Fig. A-3. Detailed flow chart for atmospheric conditions.

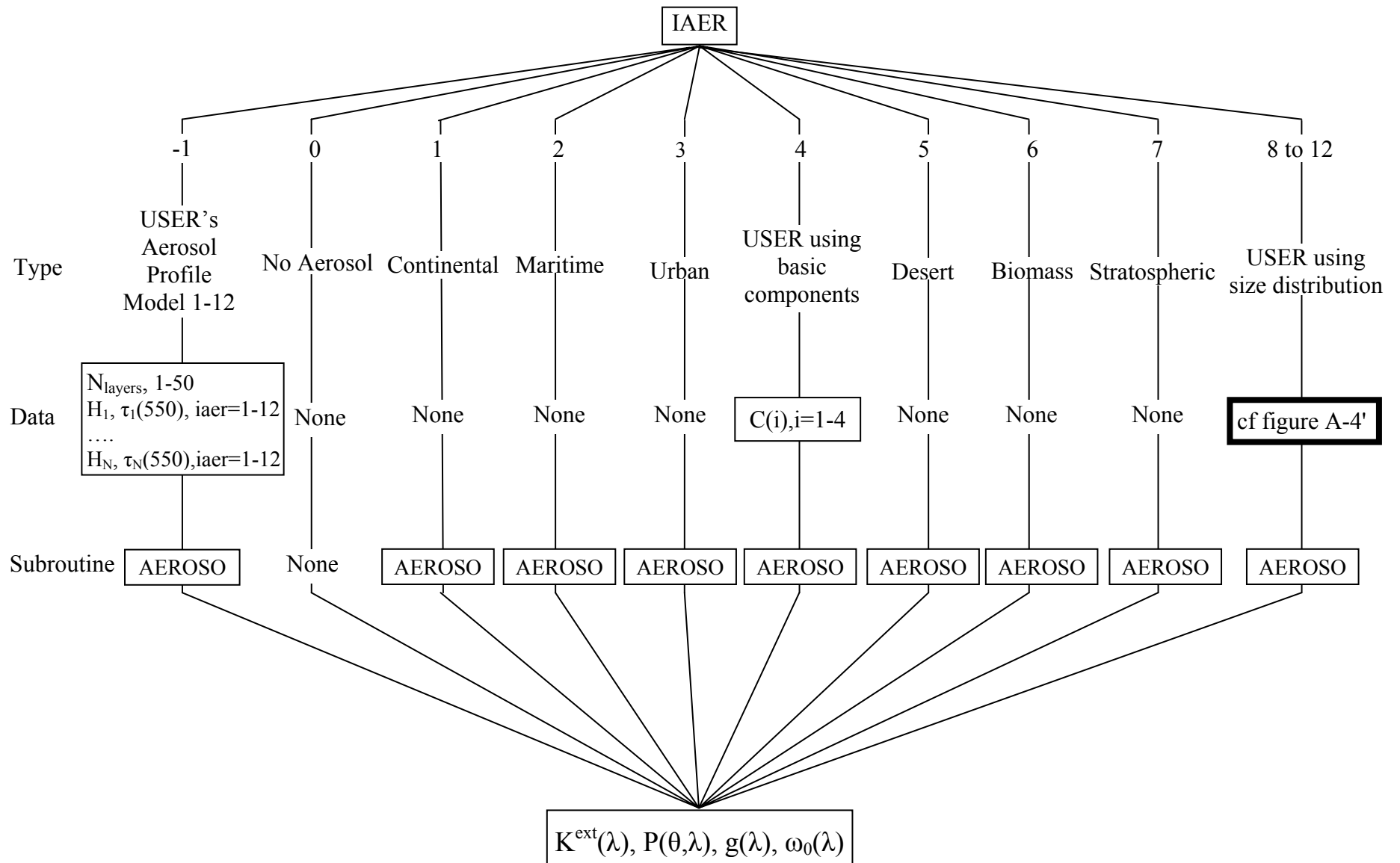


Fig. A-4. Detailed flow chart for aerosol models.

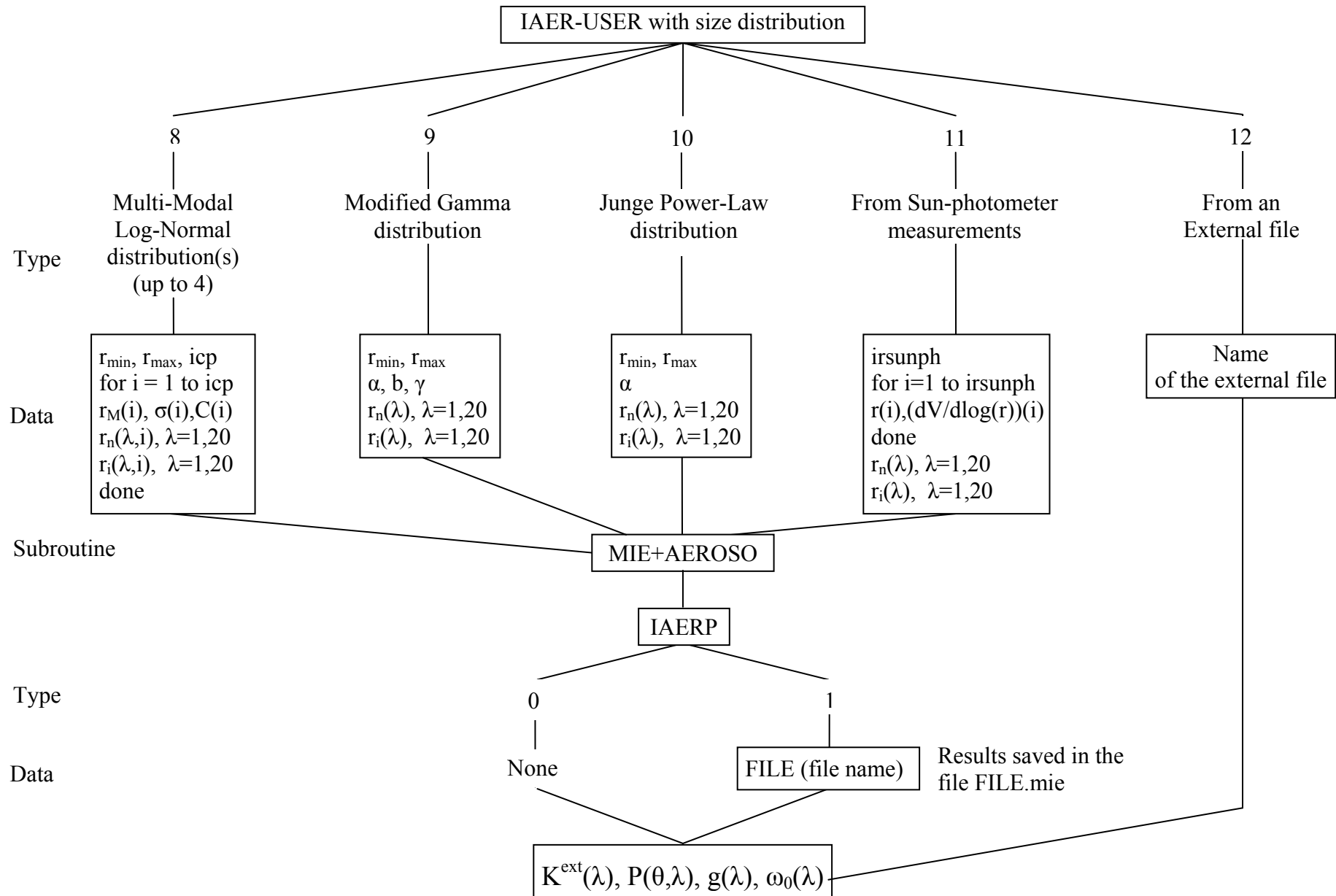


Fig. A-4'. Detailed flow chart for aerosol models (continuation).

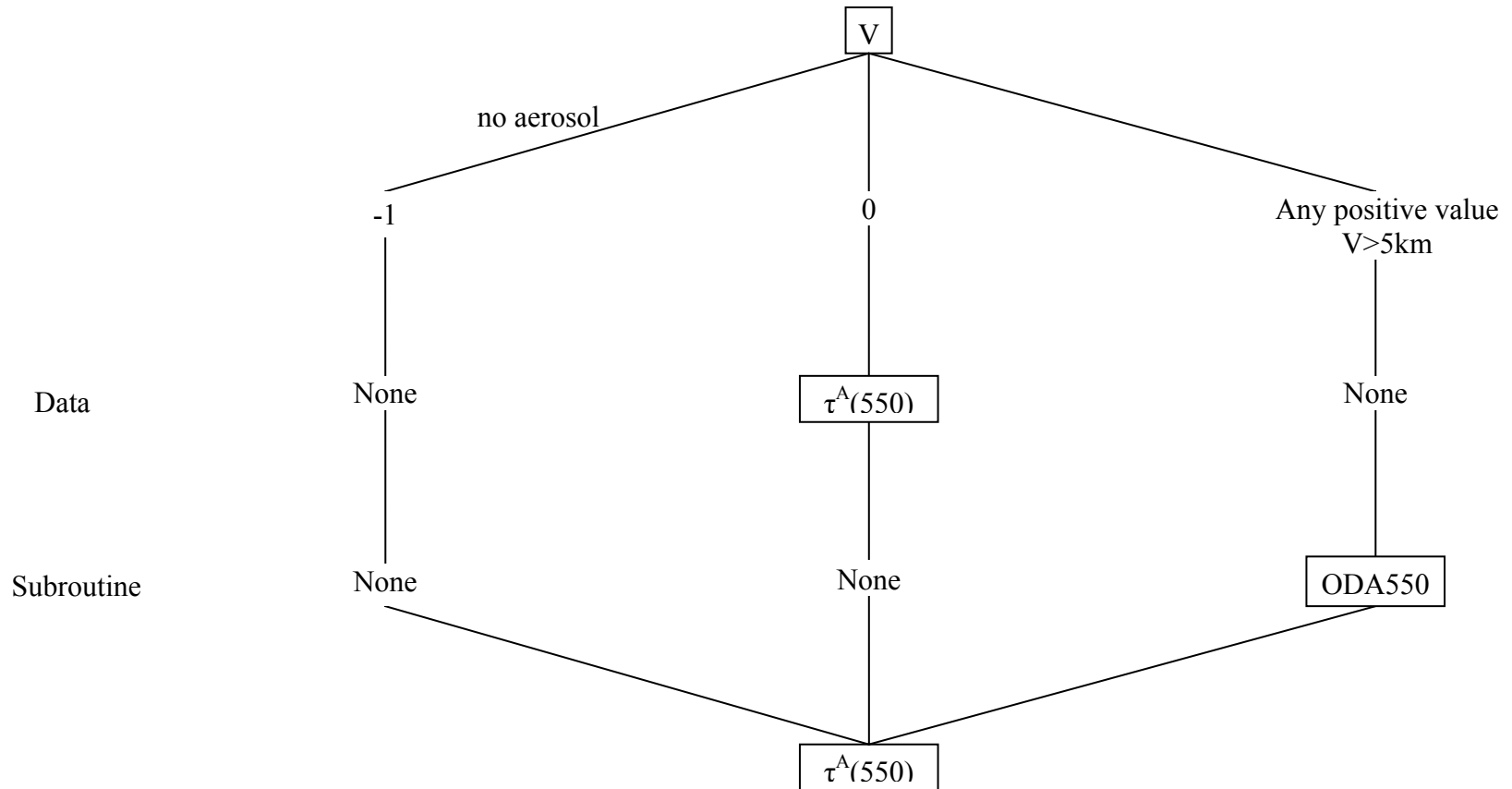


Fig. A-5. Detailed flow chart for aerosol concentration ($\tau^A(550)$, default profile).

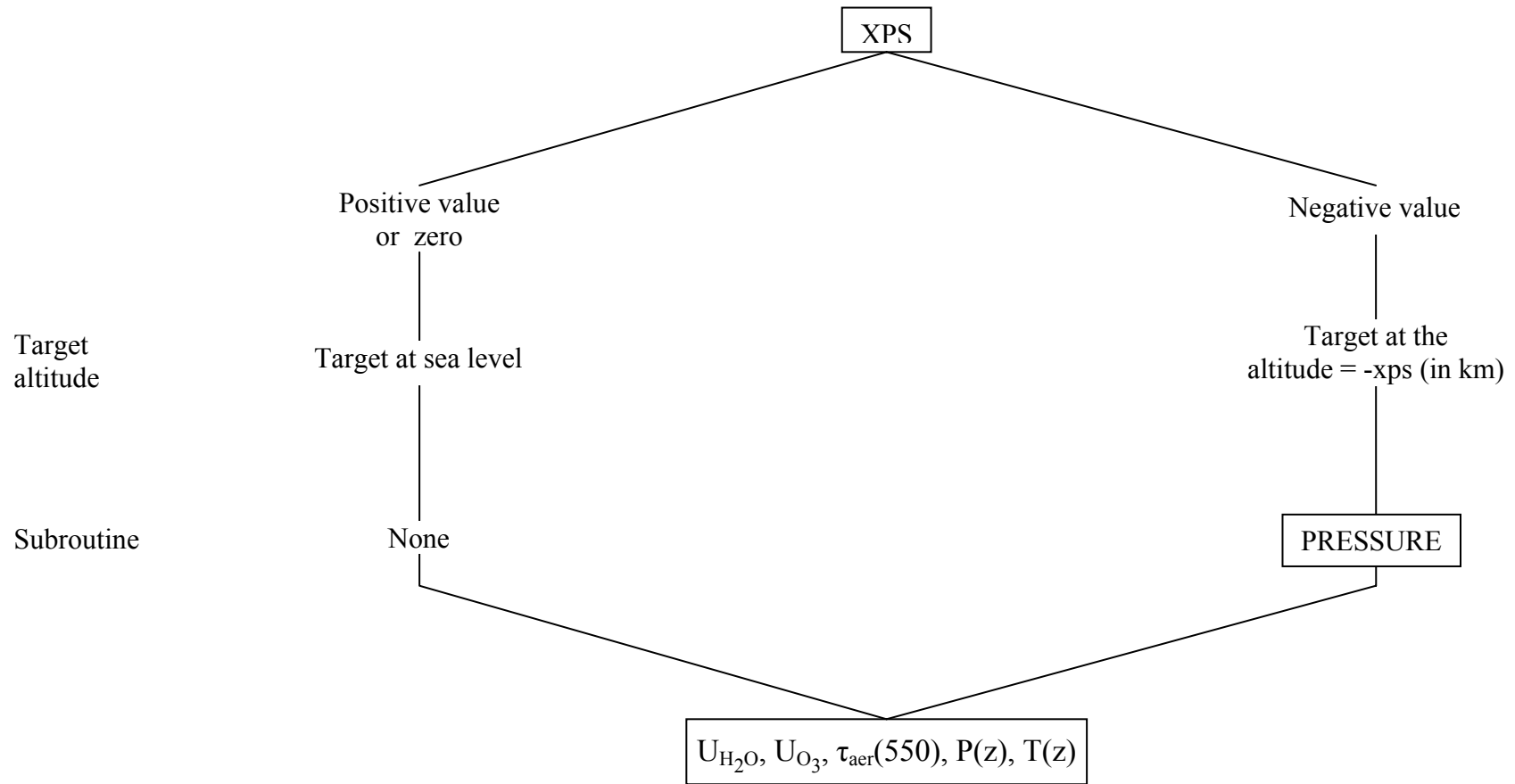


Fig. A-6. Detailed flow chart for the effect of altitude: Target.

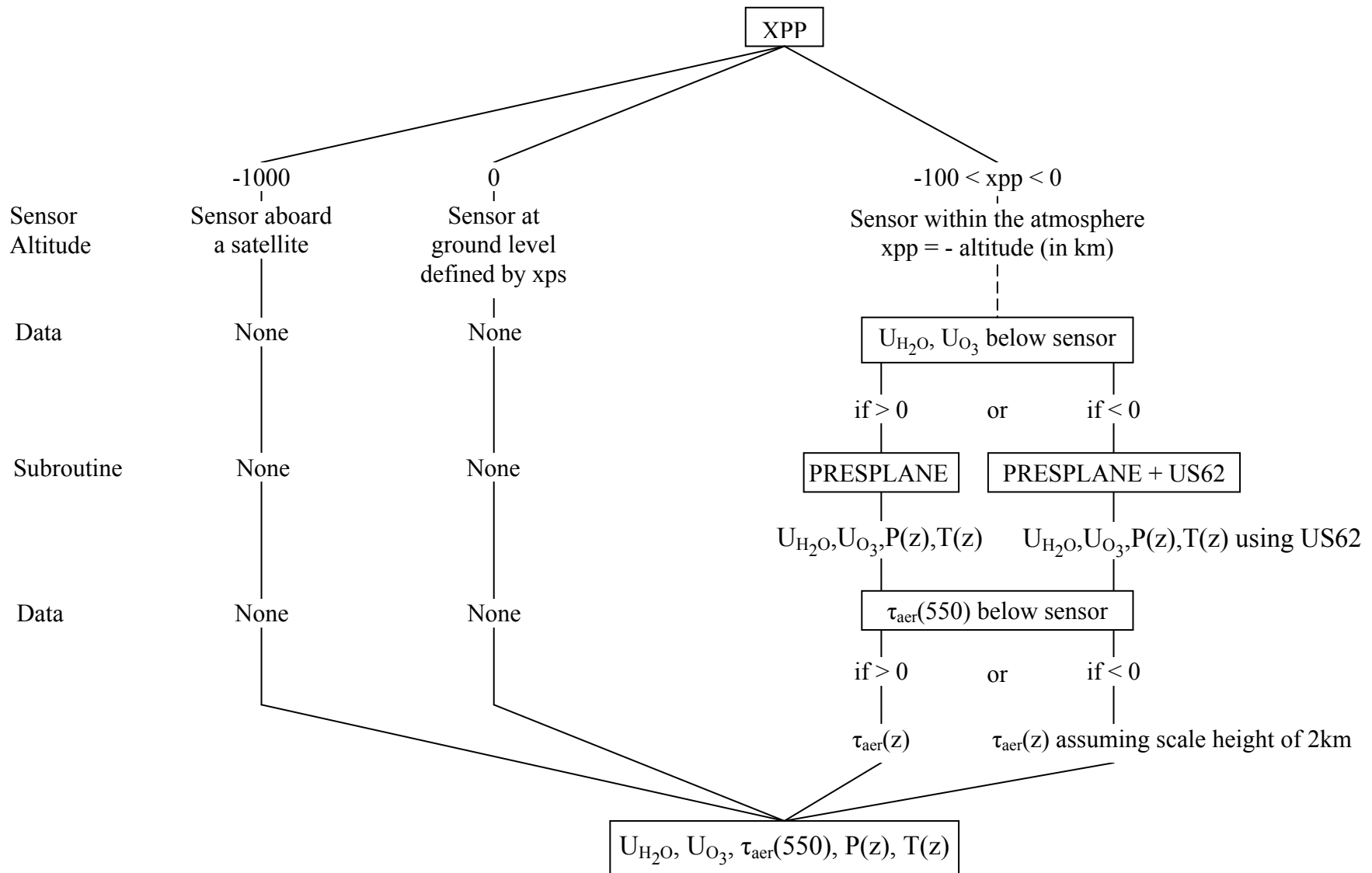


Fig.A-6'. Detailed flow chart for the effect of altitude: Sensor.

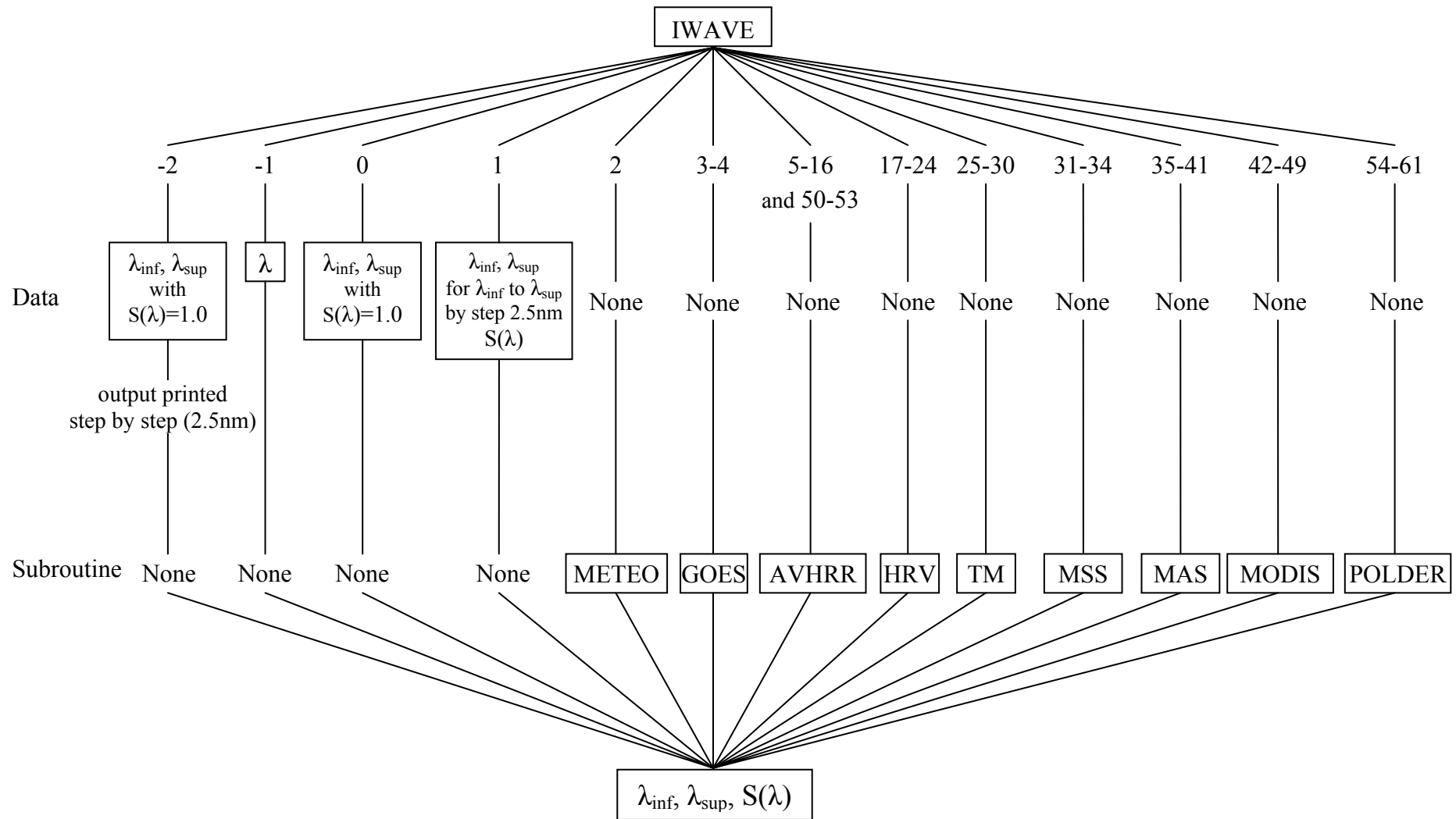


Fig. A-7. Detailed flow chart (Part I) for spectral band definition of extreme wavelengths and filter function.

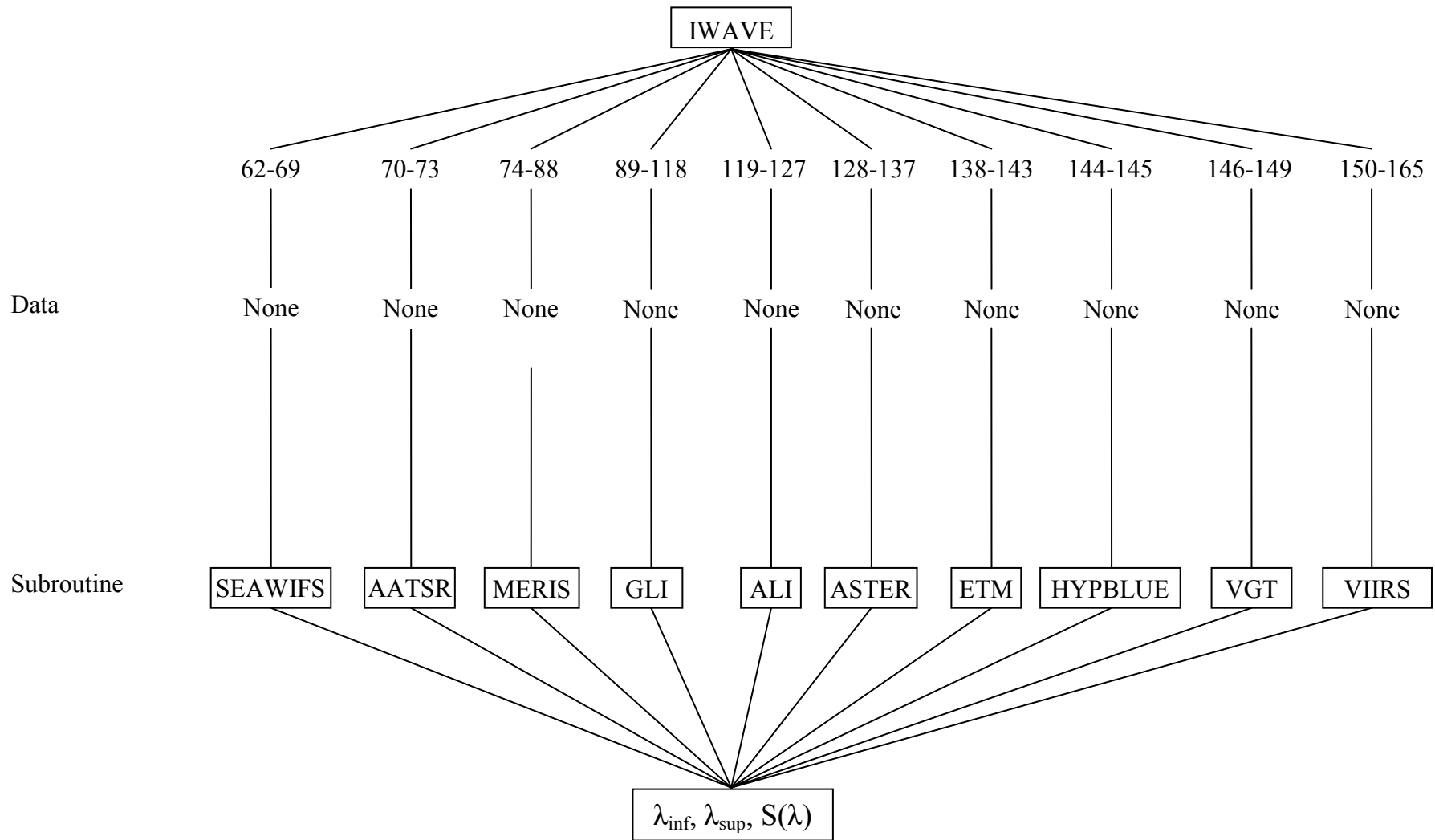


Fig. A-7'. Detailed flow chart (Part II) for spectral band definition of extreme wavelengths and filter function

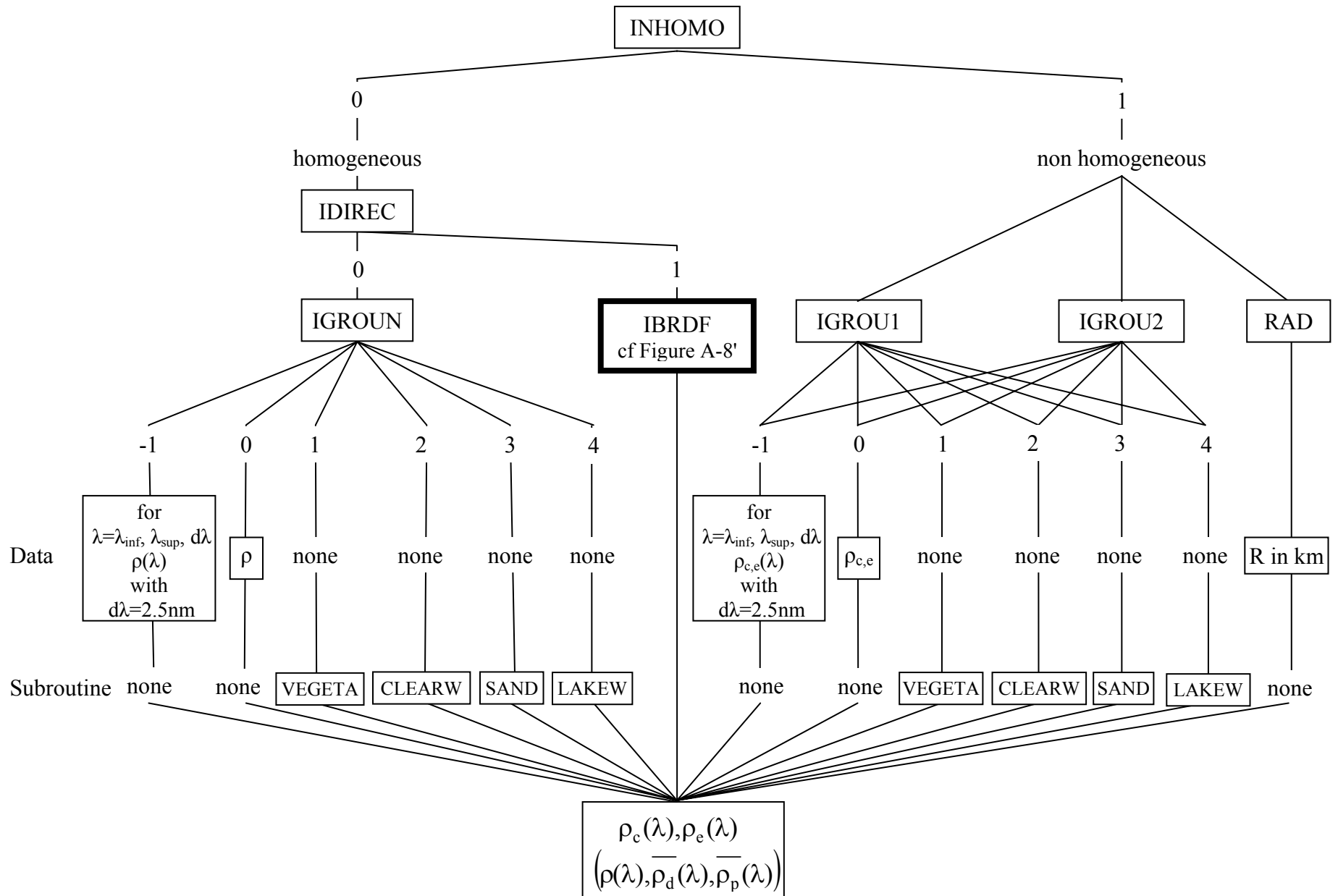


Fig. A-8. Detailed flow chart for ground reflectance, definition of the target and environment reflectances.

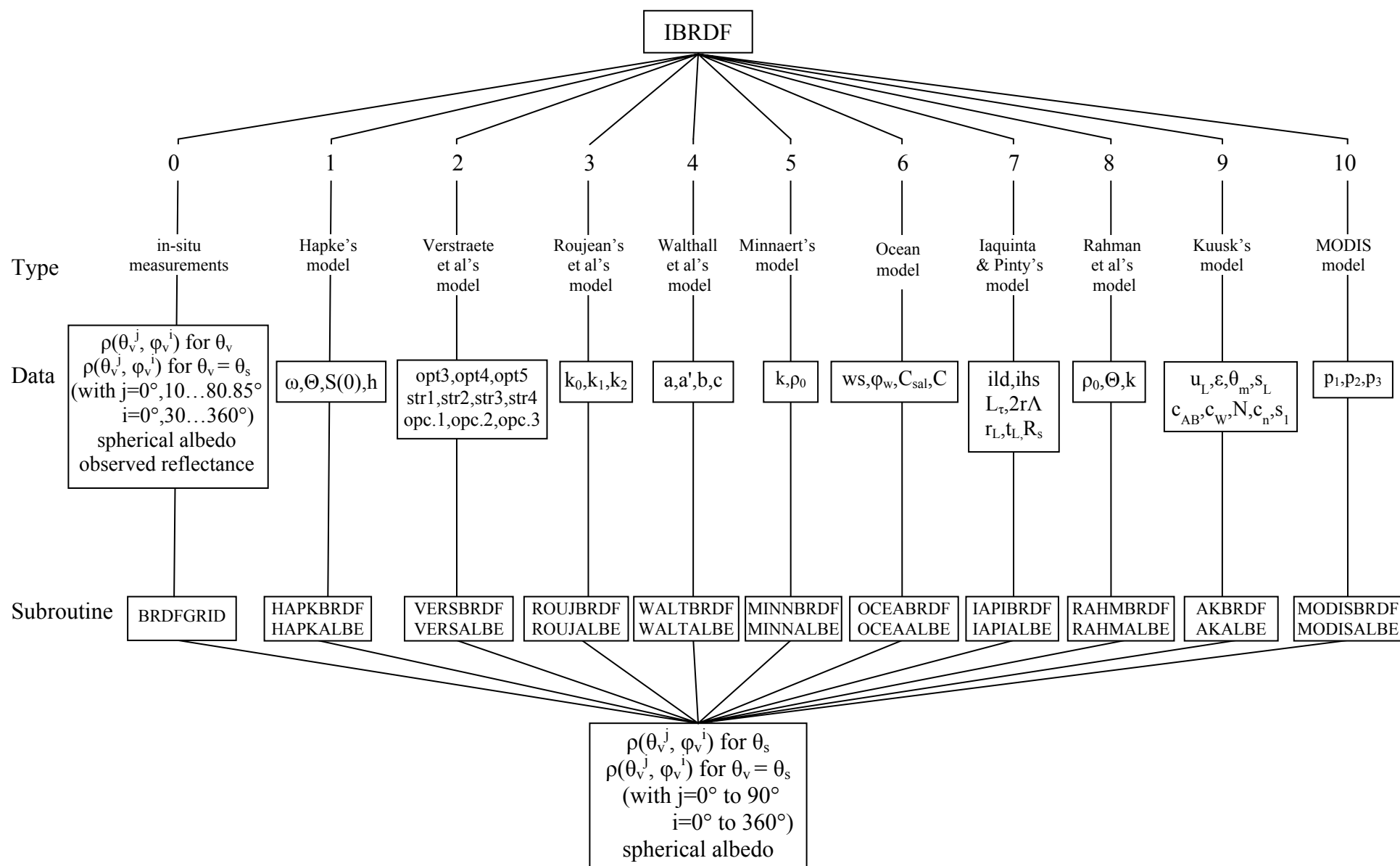


Fig. A-8'. Detailed flow chart for BRDF.

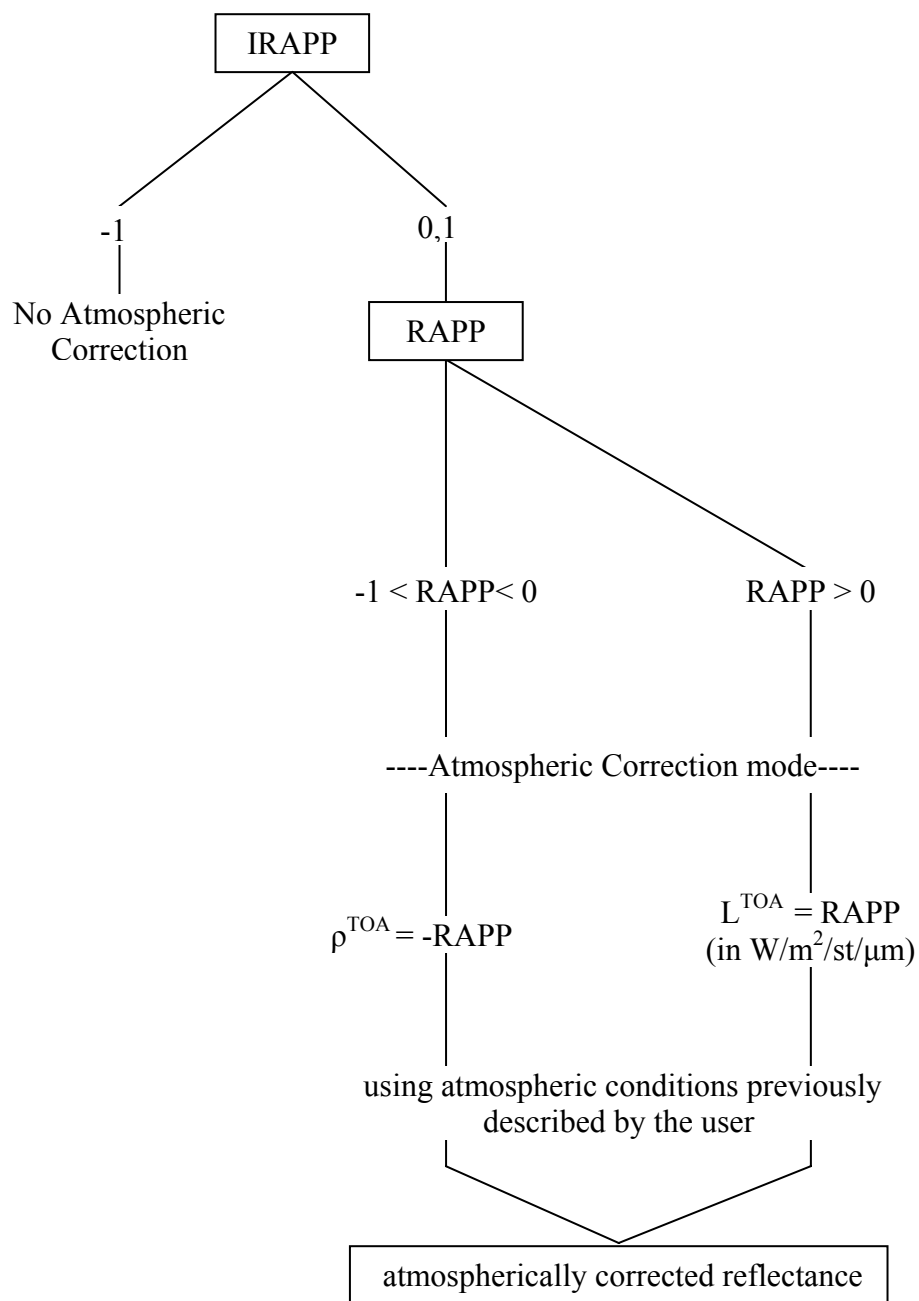


Fig. A-9. Detailed flow chart for atmospheric correction mode.

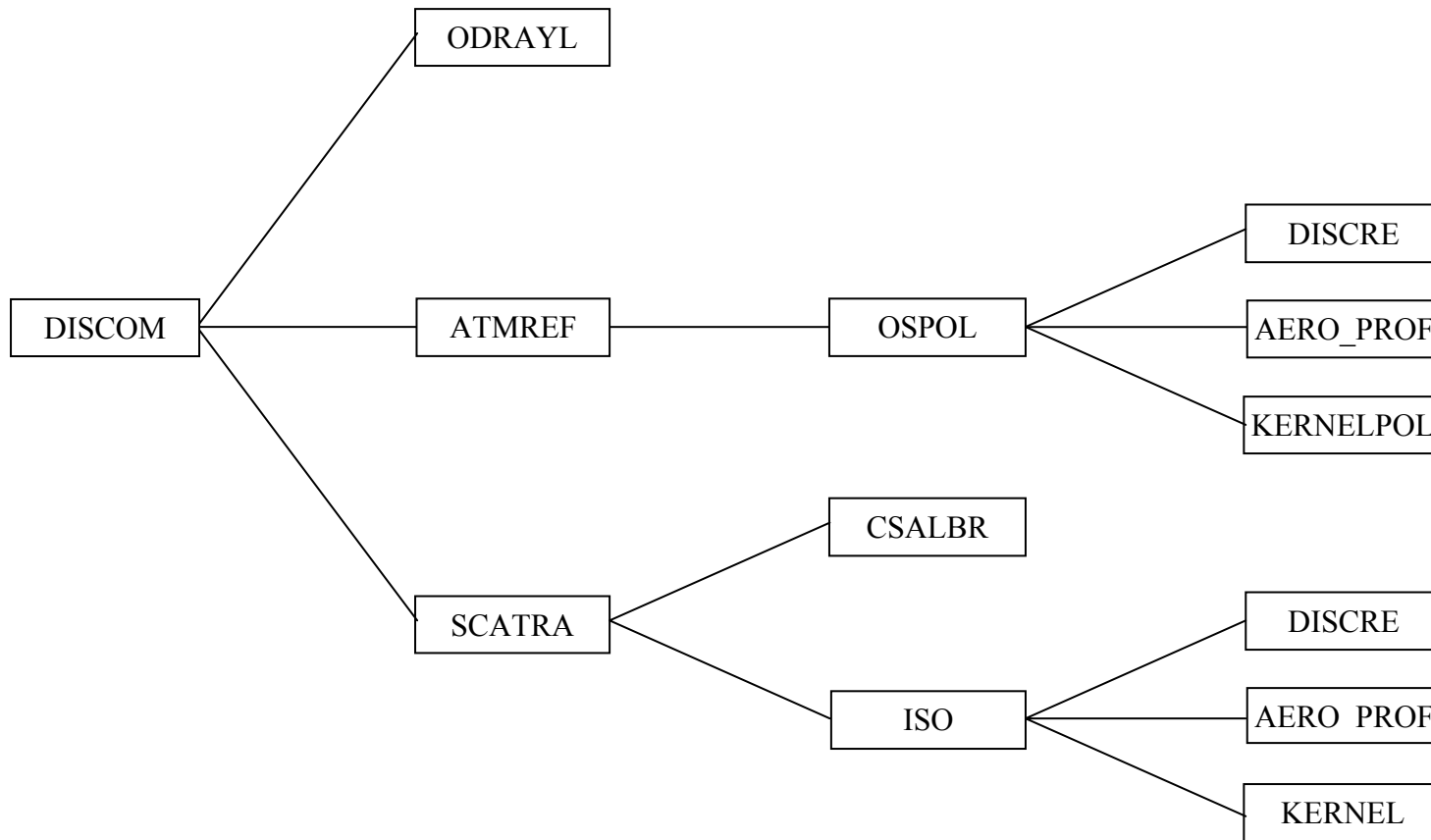


Fig. A-10. Detailed flow chart for discrete computations of the scattering atmospheric functions, ρ , $T(\theta)$, and S .

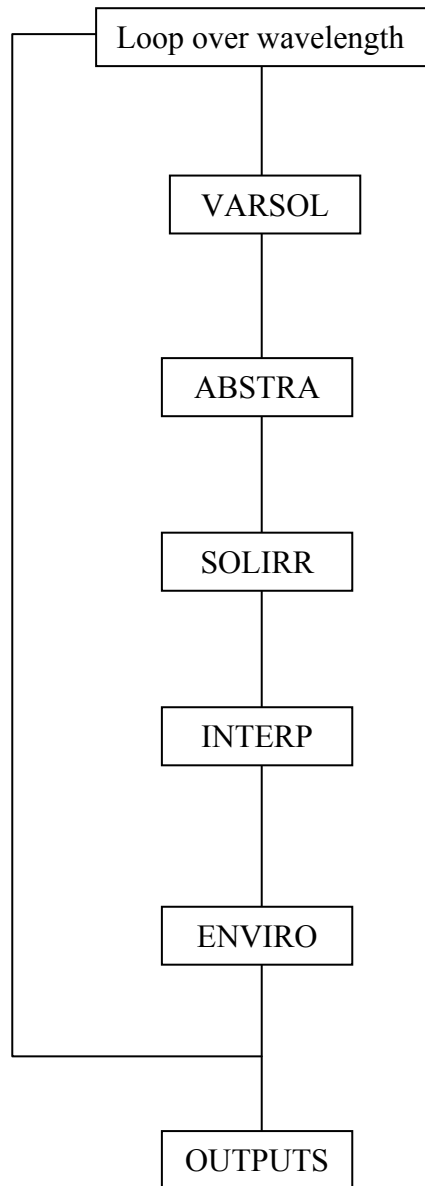


Fig A-11. Detailed flow chart for spectral integration.

INTEGRATED VALUES OF

| apparent reflectance | apparent radiance | total gaseous transmittance |
|---|---|---|
| $I_{app} = \frac{\int S(\lambda) E_{\lambda} \mu_s \rho'_{\lambda} d\lambda}{\int S(\lambda) E_{\lambda} \mu_s d\lambda}$ | $\frac{1}{\pi} \frac{\int S(\lambda) E_{\lambda} \mu_s \rho'_g d\lambda}{\int S(\lambda) d\lambda}$ | $\frac{\int S(\lambda) E_{\lambda} \mu_s T_g^{\lambda} d\lambda}{\int S(\lambda) E_{\lambda} \mu_s d\lambda}$ |

COUPLING AEROSOL – WATER VAPOR

| water vapor above aerosols | water vapor mixed with aerosols | water vapor under aerosols |
|--|---|--|
| $\frac{\int S(\lambda) E_{\lambda} \mu_s \rho_{\lambda}^{(1)} d\lambda}{\int S(\lambda) E_{\lambda} \mu_s d\lambda}$ | $\frac{\int S(\lambda) E_{\lambda} \mu_s \rho'_{\lambda} d\lambda}{\int S(\lambda) E_{\lambda} \mu_s d\lambda}$ | $\frac{\int S(\lambda) E_{\lambda} \mu_s \rho_{\lambda}^{(2)} d\lambda}{\int S(\lambda) E_{\lambda} \mu_s d\lambda}$ |

With:

| | | |
|---|--|--|
| $\rho_{\lambda}^{(1)} = \frac{T_g^{\lambda}}{T_{g_{U_{H_2O}}}^{\lambda}} \left(\rho_{R+A} + (\rho_{R+A} - \rho_R) T_{g_{U_{H_2O}}}^{\lambda} + \rho_s^* \right)$ | $\rho'_{\lambda} = \frac{T_g^{\lambda}}{T_{g_{U_{H_2O}}}^{\lambda}} \left(\rho_{R+A} + (\rho_{R+A} - \rho_R) T_{g_{U_{H_2O}}}^{\lambda} + \rho_s^* \right)$ | $\rho_{\lambda}^{(2)} = \frac{T_g^{\lambda}}{T_{g_{U_{H_2O}}}^{\lambda}} \left(\rho_{R+A} + \rho_s^* \right)$ |
| where: $\rho_s^* = T^{\downarrow}(\theta_s) T^{\uparrow}(\theta_v) \frac{\rho_s}{1 - s \rho_s} T_{g_{U_{H_2O}}}^{\lambda}$ | | |

INTEGRATED VALUES OF

| apparent polarized reflectance | apparent polarized radiance |
|---|---|
| $I_{app}^{pol} = \sqrt{(Q_{app})^2 + (U_{app})^2}$ | $\frac{1}{\pi} \frac{I_{app}^{pol} \cdot \int S(\lambda) E_{\lambda} \mu_s d\lambda}{\int S(\lambda) d\lambda}$ |
| direction of the plane of polarization | total polarization ratio |
| $\frac{1}{2} \arctan \left(\frac{U_{app}}{Q_{app}} \right)$ | $\frac{I_{app}^{pol}}{I_{app}}$ |
| <p>where:</p> $Q_{app} = \frac{\int S(\lambda) E_{\lambda} \mu_s q d\lambda}{\int S(\lambda) E_{\lambda} \mu_s d\lambda}, \quad U_{app} = \frac{\int S(\lambda) E_{\lambda} \mu_s u d\lambda}{\int S(\lambda) E_{\lambda} \mu_s d\lambda}$ <p>$q \equiv q(\theta_s, \theta_v, \varphi_s, -\varphi_v, \lambda), \quad u \equiv u(\theta_s, \theta_v, \varphi_s, -\varphi_v, \lambda)$</p> | |

Fig. A-12(1). Description of the outputs.

INTEGRATED NORMALIZED VALUES OF
Irradiance at ground level

| direct irradiance | diffuse irradiance | environment irradiance |
|--|--|--|
| $\frac{\int S(\lambda) E_{\lambda} \mu_s \frac{e^{-\tau/\mu_s} [1 - \langle \rho_{\lambda} \rangle s_{\lambda}] d\lambda}{T^{\lambda}(\theta_s)}}{\int S(\lambda) E_{\lambda} \mu_s d\lambda}$ | $\frac{\int S(\lambda) E_{\lambda} \mu_s \frac{t_d^{\lambda}(\theta_s) [1 - \langle \rho_{\lambda} \rangle s_{\lambda}] d\lambda}{T^{\lambda}(\theta_s)}}{\int S(\lambda) E_{\lambda} \mu_s d\lambda}$ | $\frac{\int S(\lambda) E_{\lambda} \mu_s \langle \rho_{\lambda} \rangle s_{\lambda} d\lambda}{\int S(\lambda) E_{\lambda} \mu_s d\lambda}$ |

Reflectance at satellite level

| atmosphere intrinsic reflectance | environment reflectance | target reflectance |
|--|---|---|
| $\frac{\int S(\lambda) E_{\lambda} \mu_s T_g^{\lambda}(\theta_s, \theta_v) \rho_{\lambda}^a d\lambda}{\int S(\lambda) E_{\lambda} \mu_s d\lambda}$ | $\frac{\int S(\lambda) E_{\lambda} \mu_s T g^{\lambda}(\theta_s, \theta_v) \frac{T^{\lambda}(\theta_s) t_d^{\lambda}(\theta_v) \langle \rho_{\lambda} \rangle}{1 - \langle \rho_{\lambda} \rangle s_{\lambda}} d\lambda}{\int S(\lambda) E_{\lambda} \mu_s d\lambda}$ | $\frac{\int S(\lambda) E_{\lambda} \mu_s T g^{\lambda}(\theta_s, \theta_v) \frac{T^{\lambda}(\theta_s) e^{-\tau/\mu_v} \rho_{\lambda}}{1 - \langle \rho_{\lambda} \rangle s_{\lambda}} d\lambda}{\int S(\lambda) E_{\lambda} \mu_s d\lambda}$ |

INTEGRATED ABSOLUTE VALUES OF
Irradiance at ground level(W/m²/μm)

| direct solar irradiance | Atmosphere diffuse irradiance | environment irradiance |
|---|---|---|
| $\frac{\int S(\lambda) E_{\lambda} \mu_s T_g^{\lambda}(\theta_s) e^{-\tau/\mu_s} d\lambda}{\int S(\lambda) d\lambda}$ | $\frac{\int S(\lambda) E_{\lambda} \mu_s T_g^{\lambda}(\theta_s) t_d^{\lambda}(\theta_s) d\lambda}{\int S(\lambda) d\lambda}$ | $\frac{\int S(\lambda) E_{\lambda} \mu_s T_g^{\lambda}(\theta_s) \frac{T^{\lambda}(\theta_s) \langle \rho_{\lambda} \rangle s_{\lambda}}{1 - \langle \rho_{\lambda} \rangle s_{\lambda}} d\lambda}{\int S(\lambda) d\lambda}$ |

Radiance at satellite level (W/m²/μm)

| atmosphere intrinsic radiance | environment radiance | target radiance |
|--|---|---|
| $\frac{1}{\pi} \frac{\int S(\lambda) E_{\lambda} \mu_s T_g^{\lambda}(\theta_s, \theta_v) \rho_{\lambda}^a d\lambda}{\int S(\lambda) d\lambda}$ | $\frac{1}{\pi} \frac{\int S(\lambda) E_{\lambda} \mu_s T_g^{\lambda}(\theta_s, \theta_v) \frac{T^{\lambda}(\theta_s) t_d^{\lambda}(\theta_v) \langle \rho_{\lambda} \rangle}{1 - \langle \rho_{\lambda} \rangle s_{\lambda}} d\lambda}{\int S(\lambda) d\lambda}$ | $\frac{1}{\pi} \frac{\int S(\lambda) E_{\lambda} \mu_s T_g^{\lambda}(\theta_s, \theta_v) \frac{T^{\lambda}(\theta_s) e^{-\tau/\mu_v} \rho_{\lambda}}{1 - \langle \rho_{\lambda} \rangle s_{\lambda}} d\lambda}{\int S(\lambda) d\lambda}$ |

| integrated function filter (in μm) | | integrated Solar Spectrum (in W/m ²) |
|------------------------------------|--|--|
| $\int S(\lambda) d\lambda$ | | $\int S(\lambda) E_{\lambda} d\lambda$ |

Fig. A-12(2). Description of the outputs.

| | DOWNWARD | UPWARD | TOTAL |
|---|---|---|---|
| Gas Trans: H ₂ O, O ₃ , CO ₂ , O ₂ N ₂ O, CH ₄ , CO | $\frac{\int S(\lambda) \mu_s E_\lambda \prod_{i=1}^7 T g_i^\lambda(\theta_s) d\lambda}{\int S(\lambda) \mu_s E_\lambda d\lambda}$ | $\frac{\int S(\lambda) \mu_s E_\lambda \prod_{i=1}^7 T g_i^\lambda(\theta_v) d\lambda}{\int S(\lambda) \mu_s E_\lambda d\lambda}$ | $\frac{\int S(\lambda) \mu_s E_\lambda \prod_{i=1}^7 T g_i^\lambda(\theta_s, \theta_v) d\lambda}{\int S(\lambda) \mu_s E_\lambda d\lambda}$ |
| Rayleigh transmittance. Aerosols transmittance. Total transmittance. | $\frac{\int S(\lambda) \mu_s E_\lambda T_\lambda(\theta_s) d\lambda}{\int S(\lambda) \mu_s E_\lambda d\lambda}$ | $\frac{\int S(\lambda) \mu_s E_\lambda T_\lambda(\theta_v) d\lambda}{\int S(\lambda) \mu_s E_\lambda d\lambda}$ | $\frac{\int S(\lambda) \mu_s E_\lambda T_\lambda(\theta_s) T_\lambda(\theta_v) d\lambda}{\int S(\lambda) \mu_s E_\lambda d\lambda}$ |

| | Rayleigh | Aerosols | Total |
|-----------------------|--|------------|-------------------|
| Spherical albedo | $\frac{\int S(\lambda) \mu_s E_\lambda S^R d\lambda}{\int S(\lambda) \mu_s E_\lambda d\lambda}$ | S^A | S^T |
| Optical depth total | $\frac{\int S(\lambda) \mu_s E_\lambda \tau^R d\lambda}{\int S(\lambda) \mu_s E_\lambda d\lambda}$ | τ^A | $\tau^A + \tau^R$ |
| Reflectance I | $\frac{\int S(\lambda) \mu_s E_\lambda \rho^R d\lambda}{\int S(\lambda) \mu_s E_\lambda d\lambda}$ | ρ^A | $\rho^R + \rho^A$ |
| Reflectance Q | $\frac{\int S(\lambda) \mu_s E_\lambda q^R d\lambda}{\int S(\lambda) \mu_s E_\lambda d\lambda}$ | q^A | $q^R + q^A$ |
| Reflectance U | $\frac{\int S(\lambda) \mu_s E_\lambda u^R d\lambda}{\int S(\lambda) \mu_s E_\lambda d\lambda}$ | u^A | $u^R + u^A$ |
| Polarized reflectance | $\sqrt{(Q^R)^2 + (U^R)^2}$ | Q^A, U^A | Q^T, U^T |

Fig. A-12(3). Description of the outputs.

| | | | |
|--|---|-----------------|---|
| Direction of the plane of polarization | $\frac{1}{2} \arctan\left(\frac{U^R}{Q^R}\right)$ | Q^A, U^A | Q^T, U^T |
| Degree of polarization | $100 \cdot \frac{\sqrt{(Q^R)^2 + (U^R)^2}}{I^R}$ | Q^A, U^A, I^A | Q^T, U^T, I^T |
| Phase function I | $\frac{\int S(\lambda) \mu_s E_\lambda P_I^R d\lambda}{\int S(\lambda) \mu_s E_\lambda d\lambda}$ | P_I^A | $\frac{\tau^R P_I^R + \tau^A P_I^A}{\tau^R + \tau^A}$ |
| Phase function Q | $\frac{\int S(\lambda) \mu_s E_\lambda P_Q^R d\lambda}{\int S(\lambda) \mu_s E_\lambda d\lambda}$ | P_Q^A | $\frac{\tau^R P_Q^R + \tau^A P_Q^A}{\tau^R + \tau^A}$ |
| Phase function U | $\frac{\int S(\lambda) \mu_s E_\lambda P_U^R d\lambda}{\int S(\lambda) \mu_s E_\lambda d\lambda}$ | P_U^A | $\frac{\tau^R P_U^R + \tau^A P_U^A}{\tau^R + \tau^A}$ |
| Primary degree of polarization | $\frac{\text{phase function } Q^R}{\text{phase function } U^R}$ | Q^A, U^A | Q^T, U^T |
| Single scattering albedo | 1.0 | ω_0^A | $\frac{\tau^R + \omega_0^A \tau^A}{\tau^R + \tau^A}$ |

Fig. A-12(4). Description of the outputs.

APPENDIX II: EXAMPLES OF INPUTS AND OUTPUTS

INPUT FILE

| | |
|---------------------------|---|
| 0 | (User-defined geometric conditions) |
| 40.0 100.0 45.0 50.0 7 23 | (SZA, SAZ, VZA, VAZ, month, day) |
| 8 | (User-defined molecular atmosphere model) |
| 3.0 3.5 | (Contents of H ₂ O-vapor (g/cm ²) & O ₃ (cm·atm)) |
| 4 | (Aerosol model) |
| 0.25 0.25 0.25 0.25 | (% of dust-like, water-soluble, oceanic, & soot) |
| 0 | (Input of aerosol opt. thickness instead of visibility) |
| 0.5 | (Aerosol optical thickness at 550 nm) |
| -0.2 | (Target at 0.2 km above the sea level) |
| -3.3 | (Aircraft at 3.3 km above the ground level) |
| -1.5 -3.5 | (H ₂ O-vapor & O ₃ under the aircraft are not available) |
| 0.25 | (Aerosol opt. thickness under the aircraft at 550 nm) |
| 11 | (AVHRR 1 (NOAA 9) Band) |
| 1 | (Non-uniform ground surface) |
| 2 1 0.5 | (Target reflect., environ. reflect., target radius (km)) |
| 1 | (Request for atmospheric correction) |
| -0.1 | (Parameter of the atmospheric correction) |
| 4 | (Ground surface is not polarized) |

OUTPUT FILE (1/3)

```

***** 6sV version 1.0B *****
*
*          geometrical conditions identity
*          -----
*          user defined conditions
*
* month:  7 day :  23
* solar zenith angle:  40.00 deg  solar azimuthal angle:  100.00 deg
* view zenith angle:  45.00 deg  view azimuthal angle:  50.00 deg
* scattering angle:  146.49 deg  azimuthal angle difference:  50.00 deg
*
*          atmospheric model description
*          -----
*          atmospheric model identity :
*          user defined water content : uh2o= 3.000 g/cm2
*          user defined ozone content : uo3 = 3.500 cm-atm
*          aerosols type identity :
*          user-defined aerosol model:
*              0.250 % of dust-like
*              0.250 % of water-soluble
*              0.250 % of oceanic
*              0.250 % of soot
*          optical condition identity :
*              visibility :  8.49 km  opt. thick. 550 nm :  0.5000
*
*          spectral condition
*          -----
*          avhrr 1 (noaa9)
*          value of filter function :
*              wl inf= 0.530 mic  wl sup= 0.810 mic
*
*          Surface polarization parameters
*          -----
*
* Surface Polarization Q,U,Rop,Chi  0.00000  0.00000  0.00000  0.00
*
*          target type
*          -----
*          inhomogeneous ground , radius of target  0.500 km
*          target reflectance :
*          spectral clear water reflectance  0.045
*          environmental reflectance :
*          spectral vegetation ground reflectance 0.129
*
*          target elevation description
*          -----
*          ground pressure [mb]  989.01
*          ground altitude [km] 0.200
*          gaseous content at target level:
*              uh2o= 3.000 g/cm2          uo3= 3.500 cm-atm
*
*          plane simulation description
*          -----
*          plane pressure [mb]  657.54
*          plane altitude absolute [km]  3.500

```

```

*           atmosphere under plane description:
*           ozone content           0.082
*           h2o   content           2.389
*           aerosol opt. thick. 550nm 0.281
*
*           atmospheric correction activated
*           -----
*           BRDF coupling correction
*           input apparent reflectance : 0.100
*
*****

```

OUTPUT FILE (2/3)

```

*****
*
*           integrated values of :
*           -----
*
*           apparent reflectance 0.0331332 appar. rad.(w/m2/sr/mic) 12.766
*           total gaseous transmittance 0.675
*
*****
*
*           coupling aerosol -wv :
*           -----
*           wv above aerosol : 0.033 wv mixed with aerosol : 0.033
*           wv under aerosol : 0.033
*
*****
*
*           integrated values of :
*           -----
*
*           app. polarized refl. 0.0015 app. pol. rad. (w/m2/sr/mic) 0.066
*           direction of the plane of polarization-27.35
*           total polarization ratio 0.044
*
*****
*
*           int. normalized values of :
*           -----
*           % of irradiance at ground level
*           % of direct irr. % of diffuse irr. % of enviro. irr
*           0.773 0.221 0.005
*           reflectance at satellite level
*           atm. intrin. ref. environment ref. target reflectance
*           0.015 0.004 0.014
*
*           int. absolute values of
*           -----
*           irr. at ground level (w/m2/mic)
*           direct solar irr. atm. diffuse irr. environment irr
*           453.572 127.012 3.163
*           rad at satel. level (w/m2/sr/mic)
*           atm. intrin. rad. environment rad. target radiance
*           5.668 1.631 5.467
*
*           int. funct filter (in mic) int. sol. spect (in w/m2)

```

```

*           0.1174545                               185.589           *
*
*****

```

OUTPUT FILE (3/3)

```

*****
*
*           integrated values of      :
*           -----
*
*           downward      upward      total
*
*   global gas. trans. :    0.68965    0.97248    0.67513
*   water   "      "   :    0.98573    0.98623    0.97592
*   ozone   "      "   :    0.70609    0.99079    0.70008
*   co2     "      "   :    1.00000    1.00000    1.00000
*   oxyg    "      "   :    0.99344    0.99533    0.99179
*   no2     "      "   :    1.00000    1.00000    1.00000
*   ch4     "      "   :    1.00000    1.00000    1.00000
*   co      "      "   :    1.00000    1.00000    1.00000
*
*
*   rayl. sca. trans. :    0.96494    0.93809    0.90520
*   aeros. sca.   "   :    0.72074    0.82101    0.59174
*   total sca.    "   :    0.69193    0.81065    0.56092
*
*
*           rayleigh      aerosols      total
*
*   spherical albedo :    0.04939    0.04934    0.06835
*   optical depth total:    0.05550    0.42021    0.47570
*   optical depth plane:    0.01848    0.23606    0.25454
*   reflectance I      :    0.01098    0.01335    0.02182
*   reflectance Q      :    0.00118    0.00039    0.00124
*   reflectance U      :   -0.00156    0.00000   -0.00176
*   polarized reflect. :    0.00195    0.00039    0.00215
*   degree of polar.   :    17.77      2.91      9.87
*   dir. plane polar.  :   -26.48      0.00     -27.37
*   phase function I   :    1.26026    0.27565    0.39051
*   phase function Q   :   -0.21911   -0.00611   -0.03096
*   phase function U   :   -1.19913   -0.15957   -0.28084
*   primary deg. of pol:   -0.17386   -0.02215   -0.07927
*   sing. scat. albedo :    1.00000    0.52284    0.57850
*
*****
*****
*
*           atmospheric correction result
*           -----
*
*   input apparent reflectance      :    0.100
*   measured radiance [w/m2/sr/mic] :    38.529
*   atmospherically corrected reflectance
*   Lambertian case :    0.22180
*   BRDF case :    0.22180
*   coefficients xa xb xc      :    0.00685  0.03885  0.06835
*   y=xa*(measured radiance)-xb; acr=y/(1.+xc*y)
*****

```